



Sea–air CO₂ fluxes in the Indian Ocean between 1990 and 2009

V. V. S. S. Sarma¹, A. Lenton², R. M. Law³, N. Metz⁴, P. K. Patra⁵, S. Doney⁶, I. D. Lima⁶, E. Dlugokencky⁷, M. Ramonet⁸, and V. Valsala⁹

¹CSIR-National Institute of Oceanography, 176 Lawsons Bay Colony, Visakhapatnam, India

²Centre for Australian Weather and Climate research, CSIRO, Marine and Atmospheric Research, Hobart, Tasmania, Australia

³Centre for Australian Weather and Climate Research, CSIRO, Marine and Atmospheric Research, Aspendale, Victoria, Australia

⁴LOCEAN-IPSL, CNRS Universite Pierre et Marie Curie 4, place Jussieu, 75252 Paris, France

⁵Research Institute for Global Change, JAMSTEC, Yokohama 236 0001, Japan

⁶Marine Chemistry and Geochemistry, Woods Hole Oceanographic Institution, Woods Hole, MA 02543-1050, USA

⁷NOAA, Earth System Research Laboratory (ESRL), Global Monitoring Division, Boulder, CO, USA

⁸Laboratoire des Sciences du Climat et de l'Environnement (LSCE), CEA/CNRS/UVSQ, Gif sur Yvette, France

⁹Indian Institute of Tropical Meteorology, Dr. Homi Bhabha Road, Pashan, Pune, India

Correspondence to: V. V. S. S. Sarma (sarmav@nio.org)

Received: 16 June 2013 – Published in Biogeosciences Discuss.: 2 July 2013

Revised: 17 September 2013 – Accepted: 26 September – Published: 6 November 2013

Abstract. The Indian Ocean (44° S–30° N) plays an important role in the global carbon cycle, yet it remains one of the most poorly sampled ocean regions. Several approaches have been used to estimate net sea–air CO₂ fluxes in this region: interpolated observations, ocean biogeochemical models, atmospheric and ocean inversions. As part of the RECCAP (REgional Carbon Cycle Assessment and Processes) project, we combine these different approaches to quantify and assess the magnitude and variability in Indian Ocean sea–air CO₂ fluxes between 1990 and 2009. Using all of the models and inversions, the median annual mean sea–air CO₂ uptake of -0.37 ± 0.06 PgC yr⁻¹ is consistent with the -0.24 ± 0.12 PgC yr⁻¹ calculated from observations. The fluxes from the southern Indian Ocean (18–44° S; -0.43 ± 0.07 PgC yr⁻¹) are similar in magnitude to the annual uptake for the entire Indian Ocean. All models capture the observed pattern of fluxes in the Indian Ocean with the following exceptions: underestimation of upwelling fluxes in the northwestern region (off Oman and Somalia), overestimation in the northeastern region (Bay of Bengal) and underestimation of the CO₂ sink in the subtropical convergence zone. These differences were mainly driven by lack of atmospheric CO₂ data in atmospheric inversions, and poor simulation of monsoonal currents and freshwater discharge in ocean

biogeochemical models. Overall, the models and inversions do capture the phase of the observed seasonality for the entire Indian Ocean but overestimate the magnitude. The predicted sea–air CO₂ fluxes by ocean biogeochemical models (OBGMs) respond to seasonal variability with strong phase lags with reference to climatological CO₂ flux, whereas the atmospheric inversions predicted an order of magnitude higher seasonal flux than OBGMs. The simulated interannual variability by the OBGMs is weaker than that found by atmospheric inversions. Prediction of such weak interannual variability in CO₂ fluxes by atmospheric inversions was mainly caused by a lack of atmospheric data in the Indian Ocean. The OBGM models suggest a small strengthening of the sink over the period 1990–2009 of -0.01 PgC decade⁻¹. This is inconsistent with the observations in the southwestern Indian Ocean that shows the growth rate of oceanic *p*CO₂ was faster than the observed atmospheric CO₂ growth, a finding attributed to the trend of the Southern Annular Mode (SAM) during the 1990s.

1 Introduction

Since the beginning of the Industrial Revolution, atmospheric carbon dioxide (CO₂) concentration has increased with time due to anthropogenic activities such as fossil fuel combustion and land use changes. These activities led to increased accumulation of CO₂ in the atmosphere from $\sim 4.0 \text{ PgC yr}^{-1}$ in 1970 to 6.8 PgC yr^{-1} in 2000 (Raupach et al., 2007) and up to 8.4 PgC yr^{-1} in 2006 (Boden et al., 2012). Of the total anthropogenic emissions, about half remain in the atmosphere, leading to warming of the globe in the recent years (IPCC, 2007), and the remaining half is stored in the ocean and on land.

The Indian Ocean is unique compared to the other two major ocean basins as it is completely closed in the north by the Indian sub-continent and connected to the tropical Pacific via the Indonesian Throughflow (ITF) in the east, and opened to other major oceans at the southern boundary (south of 44° S ; Fig. 1). The northern Indian Ocean (NIO) experiences seasonal reversals in circulation driven by monsoonal forcing (Schott and McCreary, 2001), which modulates heat and salinity transport and the biogeochemical cycling of carbon and nitrogen. This zone is one of the most productive regions in the world, accounting for 15–20% of global ocean primary productivity (e.g., Chavez and Barber, 1987; Behrenfeld and Falkowski, 1997). Many previous studies on the ocean CO₂ system in the Indian Ocean were concentrated in the northwestern Indian Ocean (Arabian Sea; e.g., George et al., 1994; Kumar et al., 1996; Goyet et al., 1998; Sarma et al., 1996, 1998, 2003) and southwestern Indian Ocean, south of 35° S (e.g., Metzl et al., 1991; Poisson et al., 1993; Metzl et al., 1995, 1998; Metzl, 2009). The northeastern region (Bay of Bengal) receives a significant amount of freshwater and is strongly stratified compared to the northwestern Indian Ocean, leading to contrasting behavior in physical processes and biogeochemical cycling (George et al., 1994). Consequently, the northeastern Indian Ocean acts as a mild net sink of atmospheric CO₂, whereas the northwestern Indian Ocean acts as a net source (Kumar et al., 1996; Sarma, 2003; Takahashi et al., 2009; Valsala and Maksyutov, 2010a; Sarma et al., 2012). The $p\text{CO}_2$ in this region shows large seasonal variations associated with the monsoonal circulation, with maxima during summer and winter and minima in the transition periods (Sarma et al., 1998, 2000, 2012; Goyet et al., 1998; Sarma et al., 2003.)

In addition to the geographical features, the atmospheric forcing of the Indian Ocean is also unique. The predominant westerly winds can be seen along the Equator in the Indian Ocean in contrast to the dominant trade winds in other tropical ocean basins. As a result of the existence of westerly winds in the tropical Indian Ocean, a flat equatorial thermocline is present in the east–west direction that leads to an absence of upwelling in the eastern tropical Indian Ocean with a west-to-east propagation of the annual cycle of

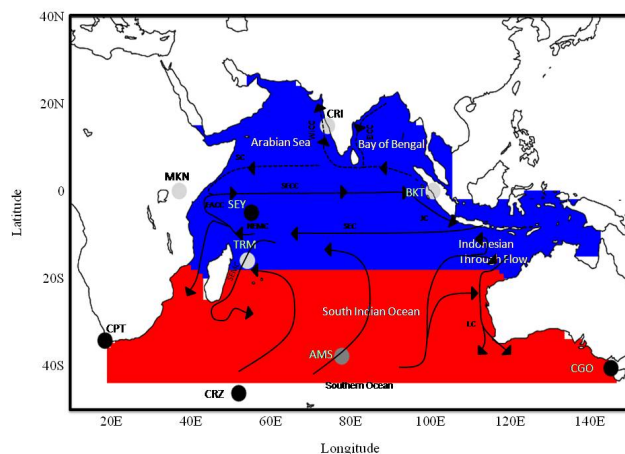


Fig. 1. Sub-regions of the Indian Ocean (30° N – 44° S , red and blue combined) used in this paper: northern Indian Ocean (blue), southern Indian Ocean (red). The water column circulation pattern is also given. East India Coastal Current (EICC), West India Coastal Current (WICC), Somali Current (SC), South Equatorial Counter-current (SECC), East African Coastal Current (EACC), northern East Madagascar Current (NEMC), southern East Madagascar Current (SEMC), South Equatorial Current (SEC), South Java Current (JC) and Leeuwin Current (LC) (Schott and McCreary, 2001). The currents shown in dashed line represent boreal winter, and these currents flow in the opposite direction during boreal summer. Overlain also is the network of atmospheric observations of CO₂ – Cape Rama, India (CRI); Mount Kenya (MKN); Bukit Koto Tabang (BKT); Seychelles (SEY); Tromelin Island (TRM); Cape Point (CPT); Amsterdam Island (AMS); Cape Grim Observatory (CGO); Crozet Island (CRZ). The color of the dot indicates how many inversions used data from that location (black: all or almost all inversions; dark grey: around half the inversions; light grey: one or two inversions). We note that the temporal period over which the atmospheric data were collected is not the same for all the stations.

SSTs (sea surface temperatures; Murtugudde and Busalacchi, 1999; Xie et al., 2002).

The southern tropical and subtropical Indian Ocean are also under the influence of water discharged from the Pacific via the Indonesian Through Flow (Valsala and Ikeda, 2007). The region between 15 to 50° S in the Indian Ocean is a major subduction zone due to positive wind stress curl (Schott et al., 2009). These subducted water masses then travel to the northern Indian Ocean through a shallow meridional overturning circulation known as the cross-equatorial cell (Miyama et al., 2003; Schott et al., 2002).

The Indian Ocean remains poorly sampled with respect to CO₂ spatially, and more importantly temporally. At present only about 30% of the region is sufficiently sampled to observationally resolve the seasonal cycle (Fig. 2). As a consequence published studies in the Indian Ocean have concentrated primarily in the northwestern (Arabian Sea; e.g., George et al., 1994; Kumar et al., 1996; Goyet et al., 1998; Sarma et al., 1998, 2003; Sarma, 2003, 2004) and southwest-

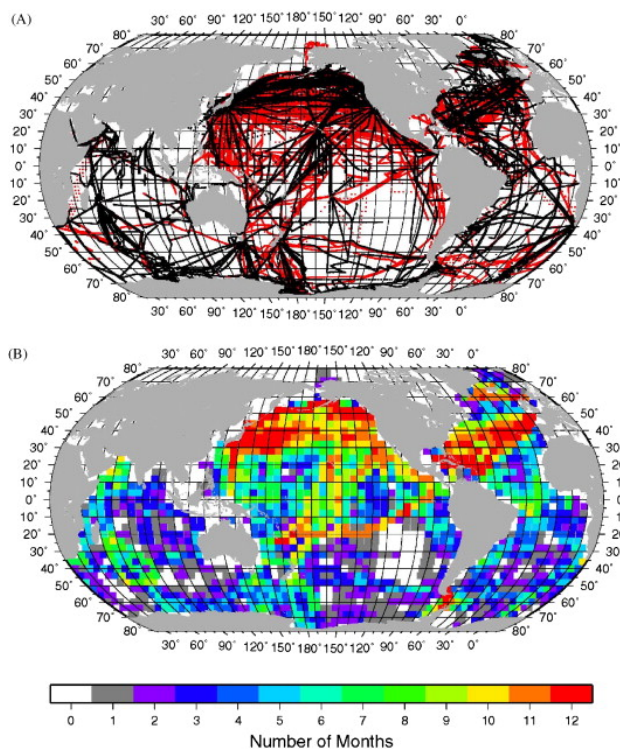


Fig. 2. The upper figure shows the location of observations of oceanic $p\text{CO}_2$ based on 3 million observations collected since 1958 (Takahashi et al., 2009). The lower panel shows the number of months of the year for which observations exist. These data are the basis of the observational data used in this study (reproduced from Takahashi et al., 2009).

ern Indian Ocean, south of 35°S (e.g., Metzl et al., 1991, 1995, 1998; Poisson et al., 1993; Metzl, 2009).

Nevertheless, several studies do focus on the entire Indian Ocean using interpolation of surface partial pressure of CO₂ ($p\text{CO}_2$), dissolved inorganic carbon (DIC) and total alkalinity (TA) data collected during the Indian Ocean cruises (e.g., Louanchi et al., 1996; Sabine et al., 2000; Bates et al., 2006). These studies suggest that the region north of 20°S acts as a strong source of CO₂ to the atmosphere (0.367PgCyr^{-1}) with a sink of atmospheric CO₂ between 20°S and 3°S of -0.13PgCyr^{-1} (Bates et al., 2006). This is in contrast with Sabine et al. (2000), who, using underway $p\text{CO}_2$ data, estimated the Indian Ocean (north of 35°S) to be a net sink of atmospheric CO₂ (-0.15PgCyr^{-1}) for the year 1995.

Recently Valsala and Makyutov (2013) estimated interannual variability in air–sea CO₂ fluxes in the NIO using a simple biogeochemical model coupled to an offline ocean tracer transport model driven by ocean reanalysis data. They found that the maximum seasonal and interannual variability in CO₂ emissions was located in the coastal Arabian Sea and southern peninsular India. Valsala et al. (2012) examined the seasonal, interannual and interdecadal variability of atmospheric CO₂ sink in the southern Indian Ocean (SIO). They

reported two distinct CO₂ uptake regions located between 15 and 35°S and between 35 and 50°S . The CO₂ response is driven by the solubility pump in the northern region, while both the solubility and biological pump contributes equally in the southern region.

The Indian Ocean also experiences strong variability driven by the Indian Ocean Dipole (IOD), and is additionally influenced by the El Niño–Southern Oscillation (ENSO) and the Southern Annular Mode (SAM) (Saji et al., 1999; Murthugude et al., 2002; Thompson and Solomon, 2002). Several physical/hydrological/circulation factors (e.g. variability in atmospheric forcings, open boundaries such as ITF; Fieux et al., 1996; Coatsanoan et al., 1999) influence sea–air CO₂ fluxes and the carbon budgets (Sarma, 2006). The estimated sea–air CO₂ fluxes at regional and basin scales suggest strong seasonal and interannual variations (Bates et al., 2006; Goyet et al., 1998; Louanchi et al., 1996; Metzl et al., 1995, 1998, 1999; Sabine et al., 2000; Sarma et al., 1998, 2003; Takahashi et al., 2002, 2009.)

Valsala and Makyutov (2013) noticed that air–sea CO₂ flux anomalies from the coastal Arabian Sea and southern peninsular India are related to the Southern Oscillation (SO) and IOD. When the correlation of CO₂ flux with the IOD is stronger, the corresponding correlation with the SO is weaker or opposite. For instance, between 1981 and 1985, about 20% of interannual variations of CO₂ emissions in the Arabian Sea were explained by IOD when SO has no significant correlation. On the other hand, between 1990 and 1995, the CO₂ emissions in the Arabian Sea displayed negative correlation with SO when IOD has no significant relation. This means that a particular mode is responsible for interannual variation over a group of years. Studies in the southwestern Indian Ocean based on long-term CO₂ observations describing the spatiotemporal $p\text{CO}_2$ variations for that region (Goyet et al., 1991; Metzl et al., 1991, 1995, 1998; Poisson et al., 1993, 1994; Metzl, 2009). In the period 1991–2007 Metzl (2009) calculated an oceanic $p\text{CO}_2$ growth rate of $2.11 \pm 0.11\ \mu\text{atm yr}^{-1}$, which is $\sim 0.4\ \mu\text{atm yr}^{-1}$ faster than in the atmosphere, suggesting that this region acts as a reducing sink of atmospheric CO₂. They further noted that the growth rate is similar between 20°S and 42°S during austral summer (2.2 – $2.4\ \mu\text{atm yr}^{-1}$), while it was lower in the north of 40°S (1.5 – $1.7\ \mu\text{atm yr}^{-1}$) than at higher latitudes ($>40^\circ\text{S}$) ($2.2\ \mu\text{atm yr}^{-1}$) during austral winter, and such spatial variations were attributed to the SAM.

Gruber et al. (2009) synthesized net air–sea CO₂ flux estimates on the basis of inversions of interior ocean carbon observations, using a suite of ocean generation circulation models and compared these with an oceanic $p\text{CO}_2$ -based climatology (Takahashi et al., 2009). This study highlighted the difficulties in simulating the seasonal dynamics of the upper ocean in the ocean biogeochemical models, resulting in a strong bias in mixed layer depth and other properties compared to observations (e.g., McKinley et al., 2006). Gruber et al. (2009) further noticed a significant mismatch

between top-down and bottom-up inversion in the tropical Indian Ocean, potentially due to a lack of atmospheric CO₂ data.

Because of the paucity of sampling in this important region, interpolated observations, atmospheric and ocean inversions, and ocean biogeochemical models have been used to quantify the response of sea–air CO₂ fluxes over the Indian Ocean. The objective of this work is to compare the sea–air CO₂ fluxes and oceanic *p*CO₂ from the different approaches to evaluate and quantify how these simulate CO₂ fluxes in the Indian Ocean on annual mean, seasonal and interannual timescales.

2 Methods

2.1 Study region

Based on the RECCAP regional definitions, we define three primary regions: (i) the entire Indian Ocean (30° N–44° S); (ii) the northern Indian Ocean (30° N–18° S); and the southern Indian Ocean (18–44° S) (Fig. 1). Additionally, beyond the RECCAP regions we define 3 sub-regions as part of the northern Indian Ocean: the Arabian Sea (0–30° N, 30–78° E); the Bay of Bengal (0–30° N, 78–100° E); and the Southern portion of the northern Indian Ocean, as each of these regions have a unique set of key drivers.

2.2 Datasets

In order to describe the regional CO₂ fluxes for the Indian Ocean and its sub-regions, RECCAP Tier 1 global CO₂ flux products were used (Canadell et al., 2011), which includes datasets from observations, ocean biogeochemical models, atmospheric and ocean inversions.

2.2.1 Observations

Overall the Indian Ocean remains one of the least sampled basins in the world ocean with respect to CO₂ measurements both in terms of space and time (Pfeil et al., 2013). Within the Indian Ocean there are only two zones where data are available: the Arabian Sea, where seasonal data are available, and southwestern Indian Ocean (near Kerguelen Islands), where longer-term data are available (Fig. 2). Away from these regions, particularly in the eastern Indian Ocean sparse sampling (2–3 times in a year) makes quantifying and understanding seasonal variability a challenge. In order to fill these gaps, Takahashi et al. (2009) compiled more than 3 million measurements of oceanic *p*CO₂ and these were averaged onto a global grid (4° × 5°) with two-dimensional advection–diffusion equations used to interpolate spatially for each month. These *p*CO₂ data have been interpolated to 1° × 1° grid and combined with the Cross-Calibrated Multi-Platform winds (CCMP; Atlas et al., 2011) to generate a monthly climatology of net sea–air CO₂ fluxes for RECCAP.

Table 1. The list of ocean biogeochemical models, the periods over which the data were evaluated and the reference to each model, and the surface area between 30° N and 44° S.

Model Name	Period	Area (km ²)	Reference
CSIRO*	1990–2009	5.06×10^7	Matear and Lenton (2008)
CCSM-BEC*	1990–2009	4.28×10^7	Thomas et al. (2008)
NEMO-Plankton5	1990–2009	5.14×10^7	Le Quéré et al. (2007)
NEMO-PISCES	1990–2009	4.67×10^7	Aumont and Bopp (2006)
CCSM-ETH*	1990–2007	4.28×10^7	Graven et al. (2012)

* Denotes the models for which *p*CO₂ values were available.

These fluxes carry several errors associated with sparse coverage of data, wind speed measurements and gas transfer coefficients (see Wanninkhof et al., 2013, and Sweeney et al., 2007, for more discussion). Following Gruber et al. (2009) and Schuster et al. (2013) we estimate the uncertainty on all sea–air flux observations to be ~50%. In our subsequent analysis and comparison with different models and inversions, we define CO₂ flux and *p*CO₂ observations as these climatologies.

2.2.2 Ocean models

Sea-to-air CO₂ flux and oceanic *p*CO₂ data were obtained from five ocean biogeochemical models coupled to ocean general circulation models (Table 1). The models represent physical, chemical and biological processes governing the marine carbon cycle and the exchange of CO₂ with the atmosphere. These models are coarse resolution and do not resolve mesoscale features. These simulations are driven with meteorological reanalysis products, based on observations, for atmospheric boundary conditions over the period 1990–2009. All of these models have been integrated from the pre-industrial period to the present day with the same atmospheric CO₂ history. The physical models vary in many aspects such as the details of physical forcing, sub-grid scale parameterizations, and experimental configurations that are detailed in the reference for each model in Table 1. In addition, the models incorporate different biogeochemical modules that can substantially influence the simulated fields of surface CO₂.

2.2.3 Atmospheric inversions

Atmospheric inversions estimate the surface CO₂ fluxes that best fit the spatiotemporal patterns of measured atmospheric CO₂ given a defined, time-evolving atmospheric transport from numerical models. Usually the atmospheric inversions include a priori information about the surface CO₂ fluxes, either from observation-based products or biogeochemical models. The atmospheric inversions used in this manuscript (Table 2) were described in Peylin et al. (2011). The inversions vary in many aspects of their configuration, but all are

run globally. Here we focus on those aspects of the inversions pertinent to estimating Indian Ocean fluxes.

While globally the atmospheric inversions typically use measurements from 50 to 100 sites, relatively few are in or near the Indian Ocean region (Fig. 1). The longest records within the region are Seychelles (55° E, 5° S) and Amsterdam Island (78° E, 38° S), while Cape Point (18° E, 34° S) and Cape Grim (145° E, 40° S) lie at the edge of the region. Cape Rama (74° E, 15° N), Bukit Kototabang (100° E, 0° S), Mt Kenya (37° E, 0° S) and Tromelin Island (54° E, 16° S) have relatively short records within the inversion period, and many inversions do not include them. Even some of the longer records have suspected data quality issues. Seychelles data before 1996 were subject to a variety of sampling methods, with samples likely taken inland between 1994 and 1996 rather than on the coast, making the 1994–1996 measurements more susceptible to local effects. Some inversions apply larger data uncertainties to Seychelles data before 1997 for this reason. Amsterdam Island measurements from 2001 to 2005 require correction for calibration issues (Le Quéré et al., 2009), but this correction is not included in most of the data products (e.g., GLOBALVIEW-CO₂, 2009) used by the inversions. Also the GLOBALVIEW-CO₂ product does not include Amsterdam Island measurements after 2005, with many inversions consequently relying on extrapolated concentrations instead. For these reasons, interannual variability from the inversions should be interpreted with caution. To account for these uncertainties in the observational record and potential resulting biases in the calculations of annual mean uptake and variability, we only use values in the period 1997–2008.

The atmospheric inversions used here estimate carbon fluxes either for pre-defined regions (8 cases) or at the resolution of the atmospheric transport model underlying the inversion (3 cases) (Table 2). The number of regions solved for varies across inversions, with 2–10 regions lying fully or partially within the Indian Ocean region analyzed here. Where only 2 Indian Ocean regions are solved for, these are close to those defined in Sect. 2.1. For inversions solving at grid-cell resolution, a correlation length scale is used to ensure that the estimated fluxes vary smoothly across larger regions. Most inversions use either the Takahashi et al. (1999) or Takahashi et al. (2009) sea–air CO₂ fluxes as a prior constraint to the inversion. These two compilations are similar for the NIO with an annual mean flux of around 0.11–0.12 PgC yr⁻¹, while in the SIO they are a little different (–0.37 or –0.49 PgC yr⁻¹). Annual mean prior fluxes for the inversions not using these compilations are similar (within 0.1 PgC yr⁻¹ of the Takahashi values).

2.2.4 Ocean inverse methods

Here we use ten ocean inverse model simulations presented by Gruber et al. (2009) and the mean value across these simulations calculated from three periods: 1995, 2000 and

2005. As this technique only solves for an annual mean state, i.e., does not resolve seasonality or interannual variability, these simulations are only used to assess the annual uptake. We have chosen to give all of the models equal weight in order to be consistent with our analysis of ocean models and atmospheric inversions, where no weighting scheme was used. The specific details on methods and models used in these ocean inversions are detailed in Mikaloff Fletcher et al. (2006, 2007) and Gruber et al. (2009).

2.3 Calculation and assessment of sea–air CO₂ fluxes

Sea–air CO₂ fluxes for ocean models and inversions were calculated as a median and the variability as a median absolute deviation (MAD; Gauss, 1816), consistent with Schuster et al. (2013) and Lenton et al. (2013). The MAD is the value where one half of all values are closer to the median than the MAD, and is a useful statistic for excluding outliers in data sets. The calculation of the annual uptake and seasonal variability of sea–air CO₂ fluxes from atmospheric inversions and ocean biogeochemical models used data from all of the models and inversions listed in Tables 1 and 2. The sea–air CO₂ flux into the ocean is defined as negative, consistent with RECCAP protocols.

3 Result and discussion

In order to examine how well ocean biogeochemical models, ocean and atmospheric inversions are simulating CO₂ uptake by the Indian Ocean with reference to observations, comparisons were made at (i) annual, (ii) seasonal and (iii) interannual timescales.

3.1 Annual mean sea–air CO₂ fluxes for 1990 to 2009

Table 3 and Fig. 3 present the median (across models and inversions) of sea–air CO₂ flux for the entire Indian Ocean (44° S–30° N), northern Indian Ocean (18° S–30° N) and southern Indian Ocean (44–18° S). For the atmospheric inversions, the annual mean is taken over the available years of each individual inversion, excluding the period before 1997 when some inversions are strongly influenced by poor-quality data at Seychelles. For ocean biogeochemical models, the annual mean was calculated over available years between 1990 and 2009, while in the case of ocean inversions the annual mean flux is calculated from the three periods 1995, 2000 and 2005. The observed pattern of annual mean uptake for the Indian Ocean is shown in Fig. 4.

3.1.1 Entire Indian Ocean (44° S–30° N)

The simulated median annual sea–air fluxes varied between –0.36 and –0.37 PgC yr⁻¹ for the Indian Ocean (Table 3 and Fig. 3), with no significant difference among methods. However, all these methods overestimate uptake by about

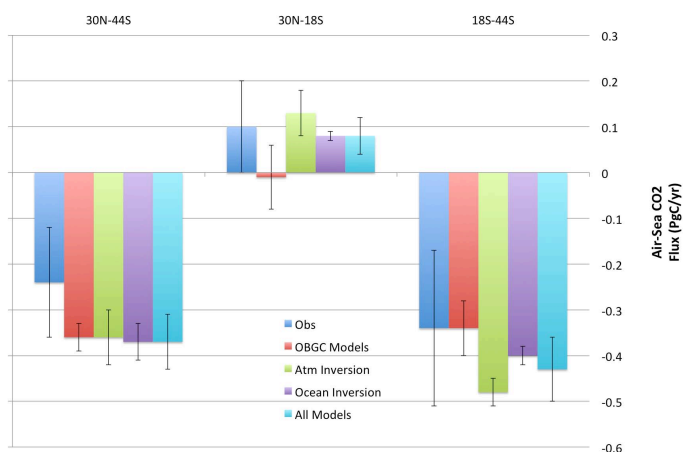
Table 2. The atmospheric inversions and periods over which data were evaluated in this study.

Model Name	Period ¹	Sites used from Fig. 1	Flux res. in Indian ²	Reference
LSCE_an_v2.1	1996–2004	5	3.75° × 2.5°	Piao et al. (2009)
LSCE_var_v1.0	1990–2008	6	3.75° × 2.5°	Chevallier et al. (2010)
C13_CCAM_low	1992–2008	5	10	Rayner et al. (2008)
C13_MATCH_rayner	1992–2008	5	8	Rayner et al. (2008)
CTRACKER_US ³	2001–2008	4	4	Peters et al. (2007)
CTRACKER_EU	2001–2008	4	4	Peters et al. (2010)
JENA_s96_v 3.3	1996–2008	3	5° × 3.75°	Rödenbeck (2005)
TRCOM_mean_9008	1990–2008	4	2	Baker et al. (2006)
RIGC_patra	1990–2008	5	4	Patra et al. (2005)
JMA_2010	1990–2008	5	2	Maki et al. (2010)
NICAM_niwa_woaia	1990–2007	6	2	Niwa et al. (2012) ⁴

¹ Period used for analysis. Inversions may have been run for longer. ² Longitude × latitude if inversion solves for each grid cell, otherwise number of ocean regions in or overlapping the Indian Ocean. ³ CT2009 release. ⁴ Inversion method as this reference, except CONTRAIL aircraft CO₂ data not used for RECCAP inversion.

Table 3. The annual multi-model median uptake (negative into the ocean) and median absolute deviation (MAD) from ocean biogeochemical models, atmospheric and ocean inversions, observations and all of the models. All units are PgC yr⁻¹.

	Obs	OBGC Models	Atm Inversions	Ocean Inversions	All Models (<i>n</i> = 26)	Surface Area (km ²)
30° N–44° S	-0.24 ± 0.12	-0.36 ± 0.03	-0.36 ± 0.06	-0.37 ± 0.08	-0.37 ± 0.06	4.9 × 10 ⁷
30° N–18° S	0.1 ± 0.05	-0.01 ± 0.07	0.13 ± 0.05	0.08 ± 0.01	0.08 ± 0.04	2.44 × 10 ⁷
18° S–44° S	-0.34 ± 0.17	-0.34 ± 0.06	-0.48 ± 0.03	-0.40 ± 0.02	-0.43 ± 0.07	2.53 × 10 ⁷

**Fig. 3.** Annual median uptake from observations, ocean biogeochemical models, atmospheric inversions and ocean inversions (PgC yr⁻¹). The error bars represent the median absolute deviation (MAD). Negative values represent fluxes into the ocean.

0.1 PgC yr⁻¹ compared to observations (-0.24 PgC yr⁻¹), but do agree within the observational uncertainty of ±0.12 PgC yr⁻¹. The observational pattern of CO₂ flux in Fig. 4 shows that the uptake is dominated by the SIO while within the NIO the air-sea flux varies in sign. The near-perfect agreement between the ocean biogeochemical models and the inversions for the entire basin is not maintained

for the NIO/SIO subdivision. The ocean inversions displayed the largest MAD in the annual uptake (0.08 PgC yr⁻¹) followed by atmospheric inversions (0.06 PgC yr⁻¹), while the smallest MAD was shown by the ocean biogeochemical models (0.03 PgC yr⁻¹; Table 3; Fig. 3). The high MAD in the inversions was caused by sparse atmospheric CO₂ measurements and differences in the modeled ocean physical circulation in the Indian Ocean.

Gruber et al. (2009) synthesized the estimates of the contemporary net air-sea CO₂ flux in the global ocean using a suite of 10 ocean general circulation models (Mikaloff Fletcher et al., 2006, 2007) and compared them with the Takahashi *p*CO₂ climatology (Takahashi et al., 2009) for the period between 1990 and 2000. The difference between the climatology and inversions at the regional level amounted to less than 0.1 PgC yr⁻¹. In addition to this the atmospheric data are available only at four stations in the Indian Ocean (Fig. 1). The reasonable agreement between atmospheric inversions and ocean *p*CO₂ estimates is mainly based on the prior estimates in the inversion of atmospheric CO₂. The deviation from these estimates should occur only if these priors turn out to be inconsistent with the atmospheric CO₂ data in the context of the inversions. The mismatches between these estimates (inversion versus observations) reflect primarily the relatively small information content of atmospheric CO₂ with regard to regional-scale air-sea CO₂ fluxes. This problem is particularly severe in the tropics and the tem-

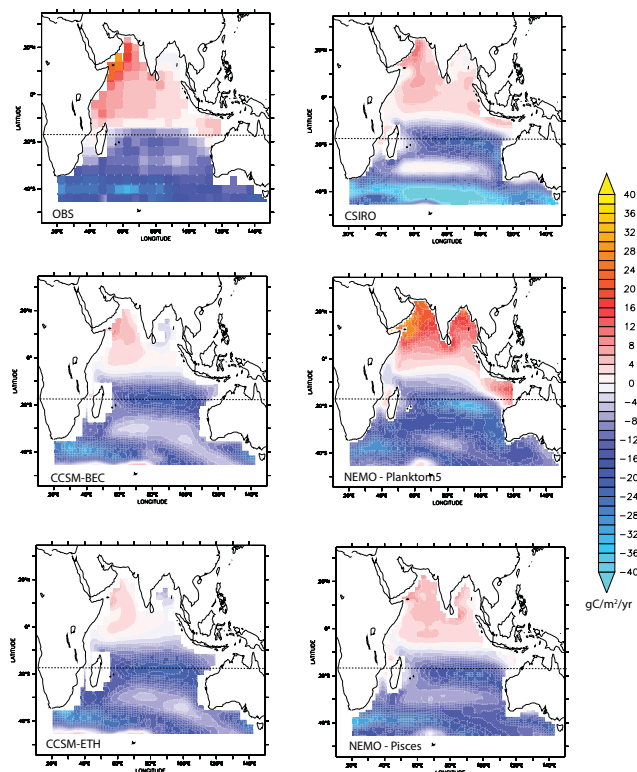


Fig. 4. Annual mean uptake, in $\text{gC m}^{-2} \text{yr}^{-1}$, from the five ocean biogeochemical models and observations; negative values reflect fluxes into the ocean.

perate Southern Hemisphere, as these regions have an inadequate number of atmospheric observation stations. As a result, small changes in the selection of the stations (Gurney et al., 2008; Patra et al., 2006) or in the setup of the inversions can lead to large shifts in the inversely estimated fluxes. The ocean regions that seem to be most affected are the tropical Indian Ocean and the temperate South Pacific. Hence, the atmospheric CO₂ inversion treats these areas as unconstrained, and may alter the estimated fluxes substantially in order to match better data constraints elsewhere.

The agreement between observations and all models in the entire basin is not maintained at several zones, namely the Oman/Somali upwelling zone, freshwater discharge zone (Bay of Bengal), the position of the South Equatorial Current (SEC), uptake in the subtropical convergence zone in the southern subtropical Indian Ocean (Fig. 4). The air-sea CO₂ fluxes were poorly simulated by many models in the northwestern Indian Ocean, where the models underestimated CO₂ fluxes to the atmosphere from the coastal upwelling zones; in contrast the ocean models overestimated the CO₂ influx in the freshwater-dominated zone in the Bay of Bengal. The SEC normally situates at 15–18° S (Schott and McCreary, 2001) which is the boundary between high surface ocean $p\text{CO}_2$ and flux to atmosphere and low surface ocean $p\text{CO}_2$ and flux into the sea (Sabine et al., 2000). This

transition zone is more easily observed in subsurface features than at the surface, marking the boundary between the low-oxygen, high-nutrient waters of the northern Indian Ocean and the high oxygen, low nutrient values of the subtropical gyre (Wyrki, 1973). This front marks the northernmost extent of the low surface $p\text{CO}_2$ values. This boundary occurred mostly north of 10° S by many models. In addition to this, the subtropical convergence zone is the most important CO₂ sink zone in the Indian Ocean, and appears underestimated by many models (Fig. 4). The more detailed examination of CO₂ fluxes in these regions is given below.

3.1.2 Northern Indian Ocean (NIO; 18° S–30° N)

Observations suggest that the ocean region north of 10° S is a net source for atmospheric CO₂, i.e., positive sea-air CO₂ flux, with the exception of the Bay of Bengal, which is a net sink of atmospheric CO₂. Encouragingly all methods, with the exception of the ocean biogeochemical models (OBGMs), simulate a positive sea-air CO₂ flux over the NIO region ($\sim 0.1 \text{ PgC yr}^{-1}$; Table 3 and Fig. 3). This net uptake is very consistent with recent water column ¹⁴C-dissolved inorganic carbon measurements analyzed over the last 2 decades ($0.1 \pm 0.03 \text{ PgC yr}^{-1}$; Dutta and Bhusan, 2012). In contrast, OBGMs suggest a small net uptake in this region ($-0.01 \pm 0.07 \text{ PgC yr}^{-1}$), but do capture areas of strong net positive flux in parts of NIO (Fig. 4). The differences in the NIO may be explained by the location of the transition from net source to sink between the NIO and SIO in OBGMs. Observationally this is located around 18° S; however all OBGMs suggest that this transition is further northward (mostly north of 10° S). This means that when the OBGM uptake estimates are integrated between 30° N and 18° S, we capture areas more characteristic of SIO conditions (i.e., strong net sink) that partially offset the positive sea-air fluxes of CO₂ in the NIO, illustrated in Fig. 5. The large source of CO₂ to the atmosphere from the Indian Ocean is driven by coastal upwelling in the northwestern Indian Ocean, i.e., off Somalia and off the Oman coast, where $p\text{CO}_2$ levels as high as $> 600 \mu\text{atm}$ have been reported during peak southwest (SW) monsoon periods (Kortzinger and Duinker, 1997; Goyet et al., 1998). All models underestimated these fluxes with the exception of NEMO-PLANKTON5, which overestimated the flux over the entire NIO. The differences in the response of the OBGMs in these key regions may be related to challenges of simulating and capturing the observed response by coarse-resolution global models, specifically the monsoonal circulation and mixing in the Arabian Sea (northwestern basin). Here the $p\text{CO}_2$ levels are highly influenced by the monsoonal circulation of atmospheric winds, and ocean circulation resulting in inputs of dissolved inorganic carbon due to vertical mixing of water column (Sarma et al., 1996, 1998; Goyet et al., 1998; Kortzinger and Duinker, 1997). It was estimated that the mixing effect is a dominant factor during the monsoon period while biological effects dominate during

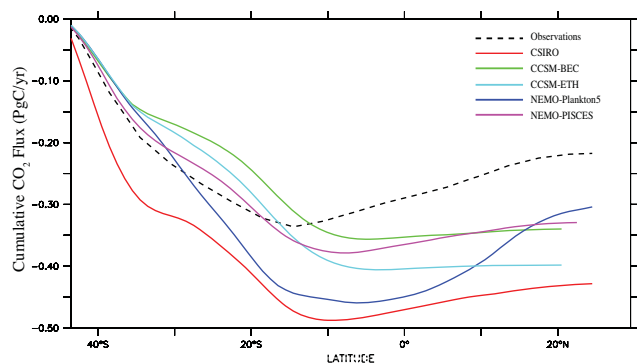


Fig. 5. The cumulative, zonally integrated, annual mean CO₂ uptake (30° N–44° S) from the biogeochemical ocean models and observations (dashed line) (PgC yr⁻¹). Negative values reflect sea–air fluxes into the ocean.

non-monsoon periods (Louanchi et al., 1996; Sarma et al., 2000). Encouragingly, OBGMs in the Arabian Sea do capture the observed net sea–air CO₂ flux, although the strength of the source varies among the models.

In contrast several of the ocean prognostic models were capable of simulating the observed CO₂ sink in the Bay of Bengal, although again the magnitude varies among models. Both NEMO-PLANKTON 5. and PISCES overestimated and changed the direction of the sea-to-atmosphere flux (Fig. 4). This is recognized as a challenging area to capture the physical and biogeochemical responses related to both the role of the monsoon and the significant amount of discharge from the major rivers such as Ganges, Brahmaputra, Godavari, etc., with variable characteristics of an inorganic carbon system. Recently Sarma et al. (2012) observed that whether coastal Bay of Bengal acts as a source or sink may depend on the characteristics of the discharge water received by the coastal zone; in many cases, the current OBGMs either do not incorporate freshwater river inputs at all or treat the lateral river boundary condition as the addition of freshwater only without incorporating explicit water chemistry (dissolved inorganic carbon, alkalinity). The OBGMs underestimated the discharge by as much as 50 % (Dia and Trenberth, 2002).

The atmospheric inversions estimate a CO₂ source to the atmosphere (0.13 ± 0.05 PgC yr⁻¹) in the NIO which is similar to that derived from observations. However it is important to note that the prior ocean flux estimates used by the inversions are also a small source with the majority between 0.11 and 0.12 PgC yr⁻¹ (range from 0.05 to 1.14 PgC yr⁻¹). Since most inversions are using only one set of atmospheric measurements in this region (Seychelles), it is likely that the prior flux has a strong influence on the estimated flux. Differences in modeled atmospheric transport are also likely to contribute. Two inversions, C13_CCAM_low and C13_MATCH_rayner, differ only by the atmospheric transport model used in the inversion and the region map for which

fluxes were solved. However in one inversion, the annual mean flux increased from the prior value and in the other it decreased. These two models show a large difference in the CO₂ response at Seychelles due to the prior land flux, and this is compensated in the inversion by altering the ocean flux local to Seychelles. This emphasizes the challenge for atmospheric inversions in this region, where both the ocean region itself has limited atmospheric observations and the surrounding land regions are also very poorly sampled, if at all.

Gruber et al. (2009) compared the “top-down” estimates of the air–sea fluxes based on the interannual inversions of atmospheric CO₂ with the “bottom-up” estimates based on the oceanic inversion or the surface ocean pCO₂ data. They found excellent agreements in many regions except the tropical Indian Ocean (18° S–18° N) and temperate Southern Hemisphere. The mismatches between these two estimates reflect information on atmospheric CO₂ with regard to air–sea CO₂ fluxes (Jacobson et al., 2007).

3.1.3 Southern Indian Ocean (SIO; 44–18° S)

This region comprises two key oceanographic regimes: the oligotrophic waters in the northern part and Southern Ocean waters in the south. The Subtropical Front (STF) separates these two regimes nominally at 40° S in this region. Integrated over these regions, the median of all approaches (-0.43 ± 0.07 PgC yr⁻¹) suggests a strong sink of atmospheric CO₂ that agrees within observational uncertainty in this region (-0.34 ± 0.17 PgC yr⁻¹). The median of OBGMs (-0.34 ± 0.06 PgC yr⁻¹) agrees particularly well with the observed CO₂ flux. Conversely the atmospheric inversions estimate a larger uptake (-0.48 ± 0.03 PgC yr⁻¹), while the oceanic inversions estimates (-0.40 ± 0.02 PgC yr⁻¹) lie between these values. It is worth noting that even the larger uptake estimated by the atmospheric and ocean inversions lies within the uncertainty of the observed flux. The SIO fluxes are similar in magnitude to the annual uptake for the entire Indian Ocean, indicating the majority of the net uptake occurs in the SIO, consistent with other studies (Sabine et al., 2000; Bates et al., 2006; Metzl, 2007; Takahashi et al., 2009).

OBGMs (Fig. 4) clearly show the response of the two oceanographic regimes: in the oligotrophic waters a net annual sink of CO₂ is evident, while south of the STF a significantly stronger net sink is seen, consistent with observations (Metzl, 2009, and references therein). However, the flux magnitudes were not well represented with reference to observations. For instance, in the 30–40° S latitudinal belt, the oceanic uptake of CO₂ was underestimated compared to the observations. Sabine et al. (1999) observed that the highest concentrations and deepest penetration of anthropogenic carbon was associated with subtropical convergence zone (30–40° S) and the transition from the high-salinity subtropical gyre waters to the low-salinity Antarctic waters. The outcropping of these density surfaces and subsequent sinking of surface waters provides a pathway for excess CO₂ to enter

the interior of the ocean. Overestimation of the CO₂ uptake by the models in these zones suggests that vertical mixing was not constrained properly in the models, leading to excess deep mixing, which resulted in an increase in surface water *p*CO₂ and a decrease in the flux to the ocean.

In the case of atmospheric inversions, there is more variation in prior flux for the SIO than for the NIO. Most inversions used a prior of either -0.37 or -0.49 PgC yr⁻¹, reflecting changes in Takahashi et al. (2009) fluxes compared with earlier compilations. The ensemble of inversions did not reconcile this difference, with estimated SIO fluxes spanning a larger range than the range of prior fluxes. As for the NIO, the SIO was poorly constrained by atmospheric measurements. The key site for the SIO region is Amsterdam Island, but this was not used in all inversions and, as noted in Sect. 2.2.3, there are some issues about data availability and calibration from 2000 onwards. It is likely that atmospheric transport differences also contributed to the variability in uptake estimates for this region. Gruber et al. (2009) noted that the temperate region of the Indian Ocean in the Southern Hemisphere (18–44° S) had excellent agreement between ocean inversions and atmospheric inversions, more so with TRANSCOM T3L3 interannually resolved inversions (Baker et al., 2006) than with TRANSCOM T3L1, which only solved for mean fluxes (Gurney et al., 2003). Though the actual reasons are unknown for why interannual inversions agreed better with the bottom-up estimates than those inversions solving only for mean fluxes or mean seasonality, they hypothesized that selection of the time period of data used and selection of observation stations were potential causes (Patra et al., 2006; Gurney et al., 2008).

3.2 Seasonal variations in *p*CO₂ and sea–air CO₂ fluxes

In order to examine how well various modeling approaches simulate seasonal variations in air–sea CO₂ fluxes with respect to observations in the Indian Ocean, the simulated *p*CO₂ by different models was compared with observations. This provides insights into the ability of ocean biogeochemical models to represent the complex interplay of physical and biological processes that drive sea–air CO₂ exchange. The ability of a model to reproduce the seasonal cycle also provides some reassurance that the ocean models are correctly projecting climate sensitivity of the processes that could influence long-term projections of the ocean CO₂ uptake.

3.2.1 Indian Ocean 44° S–30° N

In June to September, the changes in air–sea CO₂ fluxes in the Indian Ocean result from the combined effects of increased mixing driven by southwest monsoon, resulting in increased biological uptake of CO₂ in the NIO, while deeper mixing and low production, offset to some degree by surface cooling, result in a increased *p*CO₂ levels in the SIO (Louanchi et al., 1996; Sarma et al., 2000; Takahashi et al.,

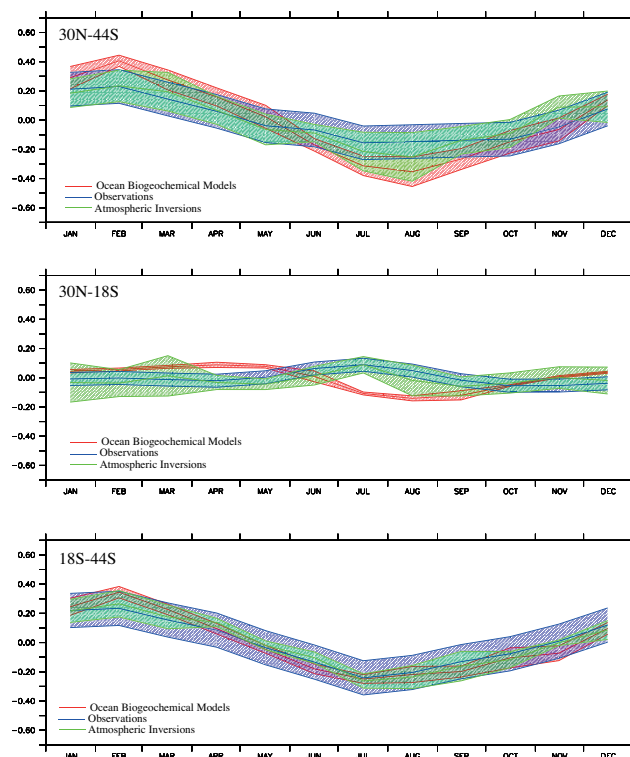


Fig. 6. Seasonal cycle anomaly of the Indian Ocean CO₂ flux (PgC yr⁻¹) from observations, ocean biogeochemical models, and atmospheric inversions for the entire Indian Ocean (30° N–44° S upper), northern Indian Ocean (30° N–18° S middle) and the southern Indian Ocean (18–44° S; lower).

2009). Figure 6 shows the median and MAD air–sea flux seasonal cycle anomaly across ocean models and atmospheric inversions compared to the seasonality derived from observations. In general the ocean models and atmospheric inversions capture the phasing of the observed seasonality for the entire Indian Ocean (Fig. 6) but overestimate the magnitude. The variation across ocean models is smaller than the variation across inversions. This variation will be explored in Sect. 3.2.2 and Sect. 3.2.3 when the seasonality of fluxes for the NIO and SIO are presented. The seasonality for the entire Indian Ocean was dominated by the seasonality in the SIO. The seasonal variations *p*CO₂ for individual OGBMs were drawn for the entire Indian Ocean in Fig. 7. Ocean biogeochemical models captured the observed seasonal cycle for the Indian Ocean; however all individual models overestimate the magnitude of the *p*CO₂ seasonality in all seasons, consistent with the larger-than-observed median annual mean uptake.

3.2.2 North Indian Ocean 18° S–30° N

The northern Indian Ocean displays strong seasonality due to occurrence of both northeast and southwest monsoons that lead to seasonal changes in atmospheric and upper ocean

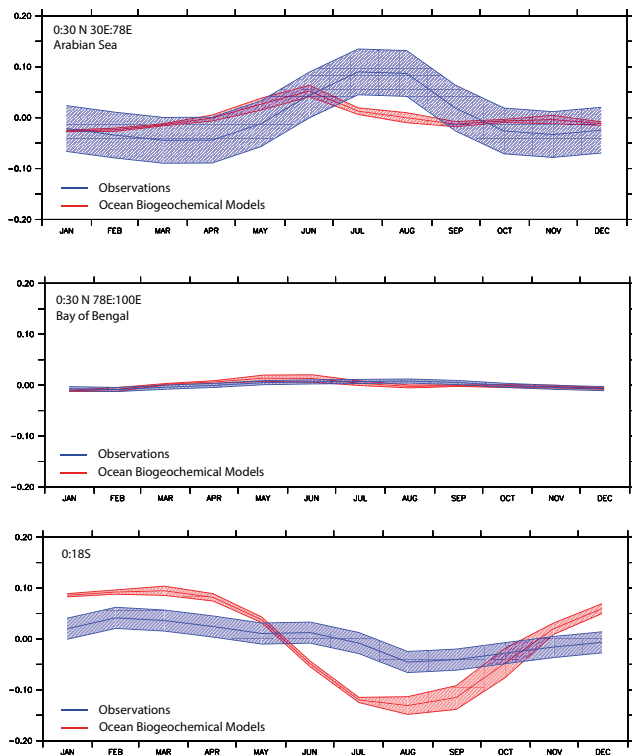


Fig. 7. Seasonal cycle $p\text{CO}_2$ anomaly of the Indian Ocean CO₂ flux (μatm) from observations and ocean biogeochemical models for total Indian Ocean (30°N – 44°S ; upper), the northern Indian Ocean (30°N – 18°S middle) and the southern Indian Ocean (18°S – 44°S ; lower).

circulation, which can have significant impact on the inorganic carbon system (George et al., 1994; Sarma et al., 1996). Figure 6 shows the spatially integrated seasonality of the NIO from atmospheric inversions and OBGMs. The observed seasonality was generally small, with observed maximum fluxes in June–August and minimum fluxes in October–December. This seasonality was mostly captured by the atmospheric inversions, but with large spread amongst inversions. By contrast, OBGMs showed a response strongly out of phase with the observations giving maximum fluxes in April–May and minimum fluxes in July–September, approximately 3–4 months ahead of the observed fluxes. Additionally, the OBGMs overestimated the magnitude of $p\text{CO}_2$ in all seasons. We will explore the behavior of the ocean models further by considering sub-regions of the NIO, while the large inversion spread will be discussed by presenting individual inversion results.

Since the NIO consists of three key sub-regions which are influenced by different combinations of physical processes (the Arabian Sea, Bay of Bengal and the equatorial Indian Ocean), the seasonal variations in sea–air CO₂ fluxes and $p\text{CO}_2$ anomaly are shown for these three zones from observations and OBGMs (Figs. 8 and 9). Observationally, it is well known that during boreal summer the flux of CO₂ to

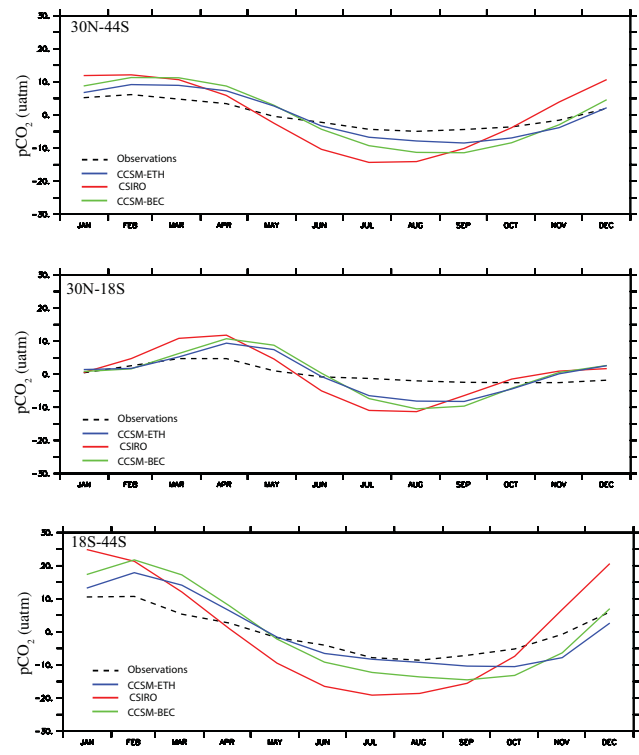


Fig. 8. Seasonal cycle CO₂ flux anomaly for parts of the northern Indian Ocean (PgC yr^{-1}) from observations and ocean biogeochemical models: the Arabian Sea (0 – 30°N , 30 – 78°E ; upper), the Bay of Bengal (0 – 30°N , 78 – 100°E ; middle) and the area between 0 and 18°S (lower).

atmosphere in the NIO results from the combined effects of the boreal summer monsoon-driven increased mixing leading to increased biological uptake of CO₂ and enhanced uptake through higher wind speeds in the NIO (Sarma et al., 2000; Takahashi et al., 2009) and the inverse during the boreal winter.

Ocean model-simulated seasonal $p\text{CO}_2$ variations in all regions were larger than observed in all three sub-regions. In the case of the Arabian Sea, the $p\text{CO}_2$ was overestimated by the models during April and June by ~ 10 – $15 \mu\text{atm}$ and underestimated during January and February by a similar magnitude (Fig. 9). These differences in $p\text{CO}_2$ are likely related to challenges of simulating the mixing and biological production in the Arabian Sea in coarse-resolution OBGMs coupled to relatively simple biogeochemical models (Friedrichs et al., 2007). However, these higher $p\text{CO}_2$ values do not translate to larger CO₂ fluxes and in fact the OBGMs significantly underestimated sea–air CO₂ fluxes in the Arabian Sea. This is because in the OBGMs the largest $p\text{CO}_2$ occurs out of phase with the monsoon, while observational $p\text{CO}_2$ phasing is closely associated with the onset of the monsoon.

The contribution of the Bay of Bengal seasonality to the total NIO seasonality is much smaller than that of the Arabian Sea, and it is consistent with ¹⁴C-based studies (e.g.,

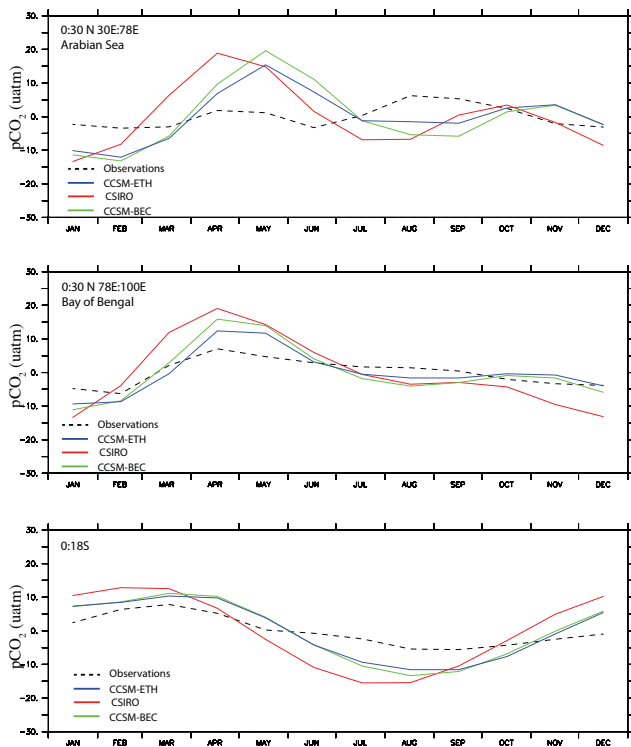


Fig. 9. Seasonal cycle $p\text{CO}_2$ anomaly for parts of the northern Indian Ocean (μatm) from observations and ocean biogeochemical models: the Arabian Sea ($0\text{--}30^\circ\text{N}$, $30\text{--}78^\circ\text{E}$; upper), the Bay of Bengal ($0\text{--}30^\circ\text{N}$, $78\text{--}100^\circ\text{E}$; middle) and the area between 0 and 18°S (lower).

Dutta and Bhushan, 2012). The ocean model seasonality is offset by several months relative to the observations, suggesting overestimation of oceanic uptake of CO₂ during boreal summer. The large $p\text{CO}_2$ values seen in April and May are captured, although overestimated in OBGMs. This overestimation leads to a sea-air positive flux earlier in the year than observed, while observations suggest a flux of similar magnitude associated with the boreal summer monsoon. In the southern equatorial region ($0\text{--}18^\circ\text{S}$), overestimation during the austral summer and underestimation during austral winter were also evident (Fig. 7) both in $p\text{CO}_2$ and sea-air CO₂ fluxes. Given that the observed uptake along the Equator is relatively small, the strong seasonality present in the OBGMs may have been associated with the inclusion of larger portion of subtropical water in the NIO region (discussed in Sect. 3.1.2).

The seasonal cycle of fluxes from individual inversions is shown in Fig. 10 for the NIO. There is a large variation across inversions. One factor in this variation is the relative uncertainty applied to any atmospheric CO₂ record and the flux being estimated. For example, an inversion with low data uncertainty and high flux uncertainty will allow the flux estimates to deviate further from any prior flux to give a better fit to the atmospheric data. This is the case for the RIGC

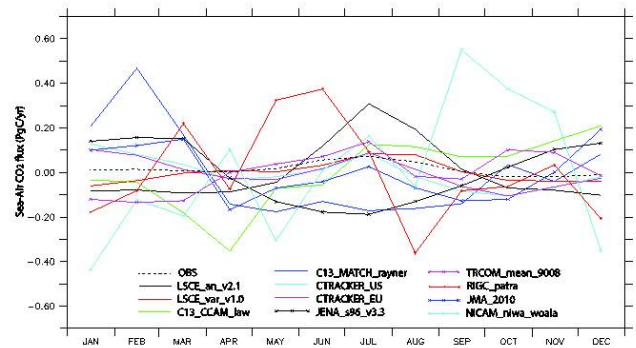


Fig. 10. The seasonal cycle of the sea-air CO₂ flux anomaly for the northern Indian Ocean ($30^\circ\text{N}\text{--}18^\circ\text{S}$) from atmospheric inversions; overlain on the plot (dashed line) is the observed seasonal cycle.

inversion, which has the largest sink in January and source in September. By contrast the LSCEv inversion uses smaller prior flux uncertainties and consequently maintains a seasonality which is much closer to the prior flux (which is close to the observed seasonality). The choice of atmospheric CO₂ data also influences the inversions. NICAM, which gives more positive fluxes in May and June than other inversions, is the only inversion to include CO₂ data from Cape Rama, India, and this may be the reason for its different seasonality. Finally, differences in atmospheric transport are also important. The large February fluxes from the MATCH inversion are a response to relatively weak transport of land biosphere seasonality to Seychelles.

3.2.3 Southern Indian Ocean (SIO; $44\text{--}18^\circ\text{S}$)

This region is comprised of the oligotrophic subtropical waters and Southern Ocean separated by the Subtropical Front. The seasonal response in this oligotrophic region is strongly solubility driven (Valsala et al., 2012) with only weak biological production evident (McClain et al., 2004) associated with vertical mixing in the winter (Louanchi et al., 1996). South of the STF in the Subantarctic Zone (SAZ), there is a well-defined seasonal cycle associated with strong biological production during the austral summer leading to a strong negative sea-air CO₂ flux. During austral winter, deep mixing brings inorganic carbon and nutrients to the surface and biological production is reduced, leading to a weaker sink of atmospheric CO₂ (Metzl et al., 2009, and references therein).

The median seasonality for the ocean biogeochemical models, atmospheric inversions and observations for the SIO are shown in Fig. 6. The similarity in the magnitude and phase with the total response was consistent across methods with this region dominating the seasonality in the sea-air flux for the entire Indian Ocean (Metzl, 2009; Takahashi et al., 2009). The simulated phase and amplitude of seasonality agreed well with observations, and suggests that the role played by the portion of the SAZ included in the SIO

is relatively small. The range in observations was generally large enough to encompass the MAD from ocean models and atmospheric inversions. For the atmospheric inversions, there is some tendency for inversions with larger seasonality to also give larger annual mean uptake in this region.

While the median of the seasonal cycle of sea–air CO₂ fluxes shows reasonable agreement with the observations, the simulated $p\text{CO}_2$ values were higher than observed. These differences may potentially be related to the different wind products used. OBGMs use the NCEP-based winds, while observations use the CCMP winds, which are weaker in this region. OBGm-simulated $p\text{CO}_2$ values were higher than observations by up to 10 μatm during austral summer and lower by up to 15 μatm during austral winter; concentrating on well-sampled regions (i.e., the southwestern Indian Ocean; Fig. 2), this difference is more pronounced during the austral summer (Fig. 7). This suggests that errors may be problems with the mixing parameterizations during the austral summer. This is consistent with observations from the GLODAP (Key et al., 2004) dataset that indicates that increasing mixing would bring subsurface water with DIC : TA ratios of (~ 0.88) to the surface acting to increase oceanic $p\text{CO}_2$.

3.3 Interannual variability (IAV)

Understanding the interannual variations in CO₂ fluxes in the Indian Ocean is an important prerequisite to projecting future CO₂ fluxes. However, at present no basin-scale observational time series are available across the Indian Ocean with which to assess simulated interannual variability of sea–air CO₂ fluxes. As a consequence, we focus on sea–air fluxes simulated from atmospheric inversions and ocean biogeochemical models. Additionally, given the fact that the Indian Ocean exhibits different regimes, we focus primarily on the IAV in the NIO between 1997 and 2008 and the SIO between 1990 and 2008. To avoid biasing the magnitude of the seasonality we first de-trend the simulated time series of IAV.

3.3.1 Indian Ocean (44° S–30° N)

The interannual variability of sea–air CO₂ fluxes from ocean biogeochemical and atmospheric inversions are shown in Fig. 11. The range of sea–air CO₂ fluxes for the period of 1990–2009 was significantly different for ocean biogeochemical models (0.02 to $-0.03 \text{ PgC yr}^{-1}$) and atmospheric inversions (-0.13 to 0.11 PgC yr^{-1}). Atmospheric inversions predicted an order of magnitude higher sea–air CO₂ flux variability. The MAD from atmospheric inversions was also significantly greater than that for the OBGMs.

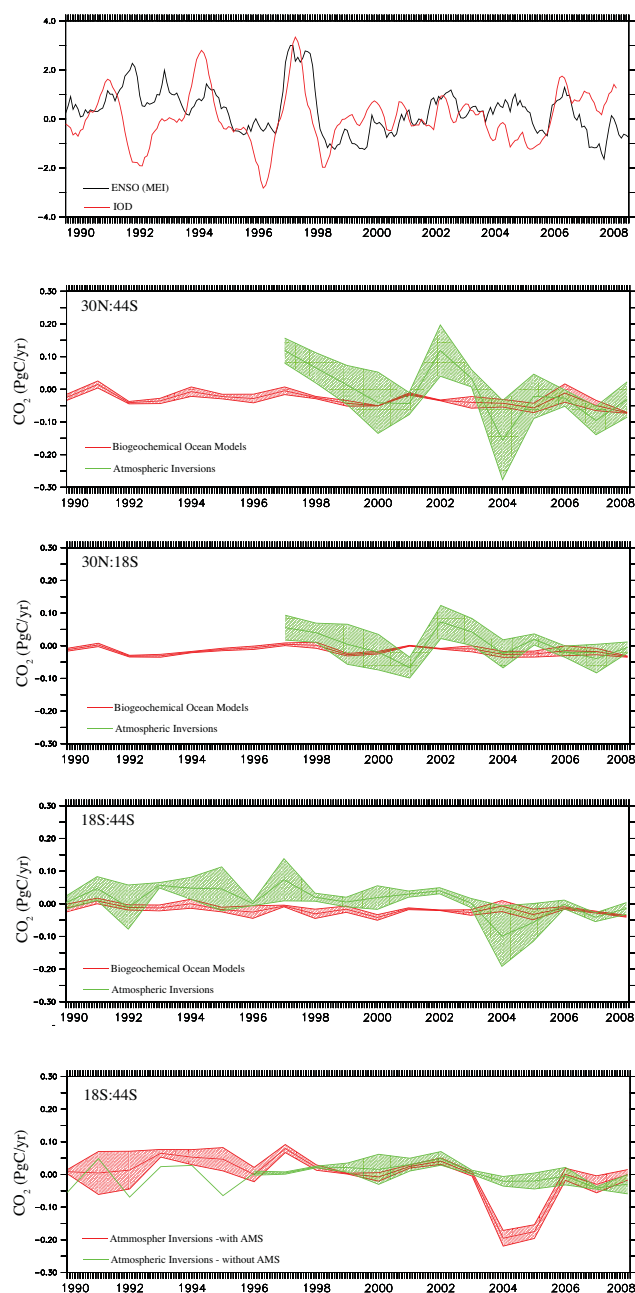


Fig. 11. The oceanic interannual variability from ocean biogeochemical models and atmospheric inversions. The upper panel shows ENSO and IOD index (the IOD/IODZM comes from FRCGC based on HADSST; the MEI comes from the ERSI (<http://www.esrl.noaa.gov/psd/enso/mei/>) that is taken from <http://climexp.knmi.nl>). The second panel represents the region 30° N–44° S, the third figure is the region 30° N–18° S, the fourth figure the region 18–44° S, and the bottom panel shows the interannual variability from atmospheric inversions in the region 18–44° S with and without the AMS data (see text for explanation).

3.3.2 Northern Indian Ocean

Although the IAV as simulated by OBGMs in the NIO was not large (-0.02 to 0.02 PgC yr⁻¹), it was larger than the annual mean uptake (1997–2009). This suggests that the character of the annual mean sink may change in OBGMs from being an area of net weak negative sea–air fluxes to weak positive sea–air fluxes. The MAD shows a very small range, suggesting that the OBGMs show good agreement at IAV timescales in this region. Atmospheric inversions give much larger median interannual variability with larger MAD than the ocean models and suggest that about 50 % of the total Indian Ocean variability occurs in the NIO. This result encompasses a large range of variability across individual inversions (0.06 to -0.07 PgC yr⁻¹), which again is larger than the annual mean uptake from inversions. Interestingly, inversions with large IAV tend also to have large amplitude seasonality and vice versa. Two reasons may contribute to this: (i) those inversions with lower variability probably used lower prior flux uncertainty for their ocean regions, thus constraining how variable these fluxes could be; and (ii) the lower variability inversions tend to be those that use the atmospheric data at the sampling time (perhaps only a few times per month for flask data), rather than as a monthly mean. Depending on the inversion setup, this might weaken the atmospheric constraint relative to the prior flux constraint.

Additionally, for the atmospheric inversions giving larger variability, there is generally some correlation between the interannual flux anomalies for the NIO and differences between Seychelles atmospheric CO₂ and measurements at a similar latitude in the Atlantic Basin (from Ascension Island). For example the below-average NIO flux in 2001 followed by the above-average flux in 2002 is coincident with a smaller SEY-ASC CO₂ difference in 2001 and larger difference in 2002. Thus the NIO flux estimates appear to be responding to local CO₂ anomalies at Seychelles. However, with little or no atmospheric data for surrounding land regions, the inversions are unable to determine whether the flux anomaly should be attributed to the NIO or to upstream land regions. It is worth noting that the Carbon Tracker inversions, which do include more recent sites from Africa and Indonesia, show weak and somewhat different IAV, supporting the hypothesis that better sampling of surrounding land regions might change the flux allocation to the NIO.

The IAV in sea–air CO₂ fluxes in the NIO has been linked to the Indian Ocean Dipole/Zonal Mode (IODZM) and the SO (Fig. 11; Valsala and Maksyutov, 2013). Valsala and Maksyutov (2013) reported that the strongest correlations (0.3) are found between the IODZM and sea–air CO₂ flux IAV in the Arabian Sea and that the roles of these two (SO and IODZM) modes are complementary in the period 1980–1999. Simulated IAV appears to show good correlation with the strong IOD event in 1997–1998, with strong positive sea–air anomalies simulated in OBGMs and inversions and low

observed biological production (Wigget et al., 2002). Over the latter period (after 2000) there appears to be some correlation with simulated fluxes over part of the record; however during some periods there is little coherence in the sign and phasing of sea–air IAV CO₂ fluxes, e.g., 2007.

3.3.3 Southern Indian Ocean

The interannual variability simulated in the SIO was small (0.02 to -0.02 PgC yr⁻¹) relative to the annual mean uptake ($\ll 10\%$). The MAD from OBGCMs is also very small in the SIO, suggesting good coherence among models at IAV timescales. Further, the magnitude of the simulated IAV was similar in the NIO and the SIO. The median of the OBGMs suggests a weak strengthening of the sink over the period 1990–2009 of -0.01 PgC decade⁻¹ ($R^2 = 0.3$). This result is inconsistent with Metzl (2009), who focused on *p*CO₂ observations in the southwestern Indian Ocean (south of 20° S). They showed that the growth rate of oceanic *p*CO₂ was faster than the observed atmospheric CO₂ growth rate, suggesting an overall reduction of the oceanic CO₂ sink in this region between 1991 and 2007. Metzl (2009) attributed this behavior to the high index state of the SAM during the 1990s. While our correlation coefficient was very low, we do note that an increase in the SAM should increase SSTs in this region (e.g., Sen Gupta et al., 2006), which would act to increase stratification and lead to a solubility-driven increase in positive sea-to-air CO₂ fluxes. These results suggest that other mechanisms may explain these trends, such as the role the IOD that plays a role in modulating SSTs in these regions (Saji et al., 1999), which is a key driver of the carbon cycle variability in the subtropical gyre.

As with the NIO, the interannual variability estimated by the atmospheric inversions was much larger than that estimated by the ocean models. The spread across atmospheric inversions was also highly variable, with some years (e.g., 2004–2005) showing much larger inversion spread than for the years immediately before or after. The range in the magnitude of IAV across inversions was slightly smaller for the SIO than the NIO, with the IAV varying between 0.05 and -0.08 PgC yr⁻¹. There was not a strong relationship across models between the magnitude of IAV for the NIO and SIO.

The key atmospheric CO₂ site for the SIO is Amsterdam Island, but not all inversions included these data. Figure 11 shows the median and MAD for the inversions grouped by whether AMS data were included. It is clear that the negative flux anomaly in 2004–2005 was driven by the AMS data. This is also the period in which there are known calibration issues with the AMS data (Le Quéré et al., 2008), which were not corrected in the GLOBALVIEW-CO₂ (2009) data compilation used by many inversions. As such, fluxes estimated through this period should be treated cautiously. Atmospheric CO₂ gradients are very small across Southern Hemisphere ocean regions, and measurement locations are remote and in harsh environments. This makes the mainte-

nance of well-calibrated measurements very challenging, but also critical for estimating interannual variability of fluxes or trends in fluxes. To illustrate this, if we calculate the trend over the period 1990–2007, we see an increasing uptake of $-0.05 \text{ PgC decade}^{-1}$ ($R^2 = 0.3$); however if we do not include AMS, we find no evidence of any trend over this period.

4 Conclusions

Despite the fact that the Indian Ocean plays an important role in the global carbon budget, it remains under-sampled with respect to surface ocean CO₂. In response to these limited observations, different approaches have been used to estimate net sea-air CO₂ exchange for the Indian Ocean and understand different scales of variability: (i) spatially interpolated observations; (ii) atmospheric inversions; (iii) ocean inversions; and (iv) ocean biogeochemical models. The goal of this study was to combine these different approaches to explore and quantify how well the models represent the variability in the uptake of sea-air CO₂ fluxes in the Indian Ocean in comparison to flux estimates derived from observations. We used the recalculated sea-air CO₂ flux climatology of Wanninkhof et al. (2013) as our observational product; five different ocean biogeochemical models driven with observed atmospheric CO₂ concentrations; twelve atmospheric inversions using atmospheric records collected around the Indian Ocean; and ten ocean inverse models driven by subsurface dissolved inorganic carbon fields.

Our results show that the median annual uptake from all four approaches applied to the entire Indian Ocean region (44° S–30° N) are between -0.24 and $-0.37 \text{ PgC yr}^{-1}$, with a median value for all models of $-0.37 \pm 0.08 \text{ PgC yr}^{-1}$. The region 44–18° S dominates the annual uptake with a median of all models of $-0.43 \pm 0.07 \text{ PgC yr}^{-1}$. Ocean inversion models show the greatest mean absolute deviation in the modeled uptake (0.08 PgC yr^{-1}). In the region north of 18° S both ocean biogeochemical models and ocean inversions show an approximately zero to small CO₂ flux (-0.01 to 0.13 PgC yr^{-1}) to the atmosphere. We see little variation in the predicted integrated flux from the entire Indian Ocean by OBGMs, atmospheric and ocean inversions.

All the models predicted the observed sea-air CO₂ flux patterns in the Indian Ocean except for underestimation of upwelling fluxes in the northwestern region (off Oman and Somalia), overestimation in the northeastern region (Bay of Bengal), and underestimation of CO₂ sink in the subtropical convergence zone. These error patterns were mainly driven by poor simulations of monsoonal currents and freshwater discharge in the case of the OBGMs.

At seasonal timescales, the observations and models capture a well-defined seasonal cycle in the sea-air CO₂ flux; however weaker amplitudes were predicted by OBGMs while stronger amplitude was found in the atmospheric in-

versions. All approaches tend to show enhanced flux into the atmosphere during summer in both the hemispheres. The seasonal variations in the ocean models were approximately 3–4 months out of phase compared with observations, with the models leading the observed maximum in the northern Indian Ocean. On the other hand, the OBGMs' simulated seasonal cycle of sea-air CO₂ fluxes agreed reasonably well with the observations, however with higher seasonal fluxes than observed. These differences may be potentially related to the different wind products used, as OBGMs used the NCEP-based winds while observations used the CCMP winds. These differences between models and observations may reflect errors in the model formulation as well as poor observational data both in the ocean and atmosphere.

The simulated interannual variability by the OBGMs is relatively weak compared to the variability derived from the atmospheric inversions and suggests that about 50% of the total Indian Ocean variability occurs in the NIO. The OBGMs suggest a weak strengthening of the sink over the period 1990–2009 of $-0.01 \text{ PgC decade}^{-1}$ in the SIO. These results are inconsistent with the observations in the southwestern Indian Ocean showing that the growth rate of oceanic *p*CO₂ was faster than the observed atmospheric CO₂ growth attributed to the SAM during the 1990s. Such controversy in interannual variations was mainly caused by lack of atmospheric observations. In order to estimate the IAV in the Indian Ocean, well-calibrated atmospheric measurements are critical, which is very challenging as these are collected in remote locations and harsh environments.

Overall the model approaches examined in this study predicted the annual ocean CO₂ uptake similarly and within the errors associated with the observations. However on the regional scale none of the models represented the observed response well due to lack of atmospheric observation and poor representation of physical processes, particularly in response to the monsoonal circulation. The future projection of the CO₂ flux from this region depends on the variations of monsoonal cycles, and on the influence of atmospheric events such as Indian Ocean Dipole Zonal Mode and El Niño. Unless these processes are represented well in the models, it will remain difficult to confidently project the future changes in CO₂ fluxes in the Indian Ocean. For this, intensive ocean observations of *p*CO₂ and more atmospheric tower observations are required for further improvement of models.

Acknowledgements. V. V. S. S. Sarma acknowledges support and encouragement from S. W. A. Naqvi, Director, CSIR-National Institute of Oceanography. A. Lenton and R. M. Law acknowledge support from the Australian Climate Change Science Program, funded by the Australian Government Department of Industry, Innovation, Climate Change, Science, Research and Tertiary Education, and by the Bureau of Meteorology and by CSIRO. S. C. Doney and I. D. Lima acknowledge support from the National Science Foundation (NSF AGS-1048827). The publication charges of this article are paid through an Asia Pacific Network grant

(#ARCP2011-11NMY-Patra/Canadell). N. Metzl acknowledges support of the EU grant 264879 CARBOCHANGE. The publication charges of this article are paid through an Asia Pacific Network grant (#ARCP2011-11NMY-Patra/Canadell). This is NIO contribution no. 5469.

Edited by: C. Sabine

References

- Atlas, R., Hoffman, R. N., Ardizzone, J., Leidner, S. M., Jusem, J. C., Smith, D. K., and Gombos, D.: A cross-calibrated, multi-platform ocean surface wind velocity product for meteorological and oceanographic applications. *B. Am. Meteorol. Soc.*, 92, 157–174, doi:10.1175/2010BAMS2946.1, 2011.
- Aumont, O. and Bopp, L.: Globalizing results from ocean in situ iron fertilization studies, *Global Biogeochem. Cy.*, 20, GB2017, doi:10.1029/2005GB002519, 2006.
- Baker, D. F., Law, R. M., Gurney, K. R., Rayner, P., Peylin, P., Denning, A. S., Bousquet, P., Bruhwiler, L., Chen, Y. H., Ciais, P., Fung, I. Y., Heimann, M., John, J., Maki, T., Maksyutov, S., Masarie, K., Prather, M., Pak, B., Taguchi, S., and Zhu, Z.: Transcom 3 inversion intercomparison: Impact of transport model errors on the interannual variability of regional CO₂ fluxes, *Global Biogeochem. Cy.*, 20, GB1002, doi:10.1029/2004GB002439, 2006.
- Bates, N., Pequignat, A. C., and Sabine, C. L.: Ocean Carbon cycling in the Indian Ocean: 1. spatiotemporal variability of inorganic carbon and air-sea CO₂ gas exchange, *Global Biogeochem. Cy.*, 20, GB3021, doi:10.1029/2005GB002492, 2006.
- Behrenfeld, M. J. and Falkowski, P. G.: Photosynthetic rates derived from satellite-based chlorophyll concentration, *Limnol. Oceanography*, 42, 1–20, 1997.
- Boden, T., Andres, B., and Marland, G.: Global CO₂ emissions from fossil fuel burning, Cement manufacture, and gas flaring, 1751–2009, CDIAC report, 20 September, 2012.
- Canadell, J. G., Ciais, P., Gurney, K., Le Quéré, C., Piao, S., Raupach, M. R., and Sabine, C.: An international effort to quantify regional carbon fluxes, *EOS.*, 92, 81–82, 2011.
- Chavez, F. P. and Barber, R. T.: An estimate of new production in the equatorial Pacific. *Deep-Sea Res.*, 34, 1229–1243, 1987.
- Chevallier, F., Ciais, P., Conway, T. J., Aalto, T., Anderson, B. E., Bousquet, P., Brunke, E. G., Ciattaglia, L., Esaki, Y., Froehlich, M., Gomez, A., Gomez-Pelaez, A. J., Haszpra, L., Krummel, P. B., Langenfelds, R. L., Leuenberger, M., Machida, T., Maignan, F., Matsueda, H., Morgui, J. A., Mukai, H., Nakazawa, T., Peylin, P., Ramonet, M., Rivier, L., Sawa, Y., Schmidt, M., Steele, L. P., Vay, S. A., Vermeulen, A. T., Wofsy, S., and Worthy, D.: CO₂ surface fluxes at grid point scale estimated from a global 21 year reanalysis of atmospheric measurements, *J. Geophys. Res.*, 115, D21307, doi:10.1029/2010JD013887, 2010.
- Coatanoan, C., Metzl, N., Fieux, M., and Coste, B.: Seasonal water mass distribution in the Indonesian throughflow entering the Indian Ocean, *J. Geophys. Res.*, 104, 20801–20826, 1999.
- Dai, A. and Trenberth, K. E.: Estimates of freshwater discharge from continents: Latitudinal and seasonal variations, *J. Hydrometeorol.*, 3, 660–687, 2002.
- Dutta, K. and Bhusahan, R.: Radiocarbon in the Northern Indian Ocean two decades after GEOSECS, *GBC*, 26, GB20218, doi:10.1029/2010GB004027, 2012.
- Fieux, M., Molcard, R., and Ilahude, A. G.: Geostrophic transport of the Pacific-Indian Oceans throughflow, *J. Geophys. Res.*, 101, 12421–12432, 1996.
- Friedrichs, M. A. M., Dusenberry, J. A., Anderson, L. A., Armstrong, R. A., Chai, F., Christian, J. R., Doney, S. C., Dunne, J., Fujii, M., Hood, R., McGillicuddy Jr., D. J., Moore, J. K., Schartau, M., Spitz, Y. H., and Wiggert, J. D.: Assessment of skill and portability in regional biogeochemical models: role of multiple planktonic groups, *JGR.*, 112, C08001, 10.1029/2006JC003852, 2007.
- George, M. D., Kumar, M. D., Naqvi, S. W. A., Banerjee, S., Narvekar, P. V., De Sousa, S. N., and Jayakumar, D. A.: A study of the carbon dioxide system in the northern Indian Ocean during premonsoon, *Mar. Chem.*, 47, 243–254, 1994.
- GLOBALVIEW-CO₂, Cooperative Atmospheric Data Integration Project Carbon Dioxide. CD-ROM, NOAA ESRL, Boulder, CO (also available on Internet via anonymous FTP to ftp.cmdl.noaa.gov, Path: ccg/co2/GLOBALVIEW), 2009.
- Goyet, C., Beauverger, C., Brunet, C., and Poisson, A.: Distribution of carbon dioxide partial pressure in surface waters of the southwest Indian Ocean, *Tellus*, 43, 1–11, 1991.
- Goyet, C., Metzl, N., Millero, F., Eiseid, G., O'Sullivan, D., and Poisson, A.: Temporal variations of pCO₂ in surface seawater of the Arabian Sea in 1995, *Deep-Sea Res. Pt. I*, 45, 609–621, 1998.
- Graven, H. D., Gruber, N., Key, R. M., Khatiwala, S., and Giraud, X.: Changing controls on oceanic radiocarbon: New insights on shallow-to-deep ocean exchange and anthropogenic CO₂ uptake, *J. Geophys. Res.-Oceans*, 117, C10005, doi:10.1029/2012JC008074, 2012.
- Gruber, N., Gloor, M., Fletcher, S. E. M., Doney, S. C., Dutkiewicz, S., Follows, M. J., Gerber, M., Jacobson, A. R., Joos, F., Lindsay, K., Menemenlis, D., Mouchet, A., Muller, S. A., Sarmiento, J. L., and Takahashi, T.: Oceanic sources, sinks, and transport of atmospheric CO₂, *Global Biogeochem. Cy.*, 23, GB1005, doi:10.1029/2008GB003349, 2009.
- Gurney, K. R., Law, R. M., Denning, A. S., Rayner, P. J., Baker, D., Bousquet, P., Bruhwiler, L., Chen, Y. H., Ciais, P., Fan, S. M., Fung, I. Y., Gloor, M., Heimann, M., Higuchi, K., John, J., Kowalczyk, E., Maki, T., Maksyutov, S., Peylin, P., Prather, M., Pak, B. C., Sarmiento, J., Taguchi, S., Takahashi, T., and Yuen, C. W.: Trans Com 3 CO₂ inversion intercomparison: 1. Annual mean control results and sensitivity to transport and prior flux information, *Tellus Ser. B.*, 55, 555–579, 2003.
- Gurney, K. R., Baker, D., Rayner, P., and Denning, S.: Interannual variations in continental-scale net carbon exchange and sensitivity to observing networks estimated from atmospheric CO₂ inversions for the period 1980 to 2005, *Global Biogeochem. Cy.*, 22, GB3025, doi:10.1029/2007GB003082, 2008.
- IPCC, Climate change 2007: the physical science basis. In: Solomon, S., Qin, D., Manning, M., Chen, Z., Marquis, M., Averyt, K. B., Tignor, M., Miller, H.L. (Eds.), Contribution of Working Group I of the Fourth Assessment Report of the Intergovernmental Panel on Climate Change. Cambridge University Press, Cambridge, United Kingdom and New York, NY, USA, 996 pp., 2007.

- Jacobson, A. R., Mikaloff Fletcher, S. E., Gruber, N., Sarmiento, J. L., and Gloor, M.: A joint atmosphere–ocean inversion for surface fluxes of carbon dioxide: 1. Methods and global-scale fluxes, *Global Biogeochem. Cy.*, 21, GB1019, doi:10.1029/2005GB002556, 2007.
- Key, R. M., Kozyr, A., Sabine, C. L., Lee, K., Wanninkhof, R., Bullister, J. L., Feely, R. A., Millero, F. J., Mordy, C., and Peng, T. H.: A global ocean carbon climatology: Results from Global Data Analysis Project (GLODAP), *Global Biogeochem. Cy.*, 18, GB4031, doi:10.1029/2004GB002247, 2004.
- Kortzinger, A. and Duinker, J. C.: Strong CO₂ emissions from the Arabian Sea during South-West Monsoon, *Geophys. Res. Lett.*, 24, 1763–1766, 1997.
- Kumar, M. D., Naqvi, S. W. A., George, M. D., and Jayakumar, D. A.: A sink for atmospheric carbon dioxide in the northeast Indian Ocean, *J. Geophys. Res.*, 101, 18121–18125, 1996.
- Lenton, A., Tilbrook, B., Law, R. M., Bakker, D., Doney, S. C., Gruber, N., Ishii, M., Hoppema, M., Lovenduski, N. S., Matear, R. J., McNeil, B. I., Metzl, N., Mikaloff Fletcher, S. E., Monteiro, P. M. S., Rödenbeck, C., Sweeney, C., and Takahashi, T.: Sea-air CO₂ fluxes in the Southern Ocean for the period 1990–2009, *Biogeosciences*, 10, 4037–4054, doi:10.5194/bg-10-4037-2013, 2013.
- Le Quéré, C., Rodenbeck, C., Buitenhuis, E. T., Conway, T. J., Langenfelds, R., Gomez, A., Labuschagne, C., Ramonet, M., Nakazawa, T., Metzl, N., Gillett, N. P., and Heimann, S.: Saturation of the Southern Ocean CO₂ sink due to recent climate change, *Science*, 319, p. 570, doi:10.1126/science.1147315, 2008.
- Le Quéré, C., Raupach, M. R., Canadell, J. G., Marland, G., Bopp, L., Ciais, P., Conway, T. J., Doney, S. C., Feely, R. A., Foster, P., Friedlingstein, P., Gurney, K., Houghton, R. A., House, J. I., Huntingford, C., Levy, P. E., Lomas, M. R., Majkut, J., Metzl, N., Ometto, J. P., Peters, G. P., Prentice, I. C., Randerson, J. T., Running, S. W., Sarmiento, J. L., Schuster, U., Sitch, S., Takahashi, T., Viovy, N., van der Werf, G. R., and Woodward, F. I.: Trends in the sources and sinks of carbon dioxide, *Nat. Geosci.*, 2, 831–836, doi:10.1038/Ngeo689, 2009.
- Louanchi, F., Metzl, N., and Poisson, A.: Modelling the monthly sea surface pCO₂ fields in the Indian Ocean, *Mar. Chem.*, 55, 265–279, 1996.
- Maki, T., Ikegami, M., Fujita, T., Hirahara, T., Yamada, K., Mori, K., Takeuchi, A., Tsutsumi, Y., Suda, K., and Conway, T. J.: New technique to analyse global distributions of CO₂ concentrations and fluxes from non-processed observational data, *Tellus B*, 62, 797–809, doi:10.1111/j.1600-0889.2010.00488.x, 2010.
- Matear, R. J. and Lenton, A.: Impact of historical climate change on the Southern Ocean carbon cycle, *J. Climate*, 21, 5820–2834, 2008.
- McClain, C. R., Signorini, S. R., and Christian, J. R.: Subtropical gyre variability observed by ocean-color satellites, *Deep Sea Res. Pt. II*, 51, 281–301, doi:10.1016/j.dsr2.2003.08.002, 2004.
- McKinley, G. A., Takahashi, T., Buitenhuis, E., Chai, F., Christian, J. R., Doney, S. C., Jiang, M. S., Lindsay, K., Moore, J. K., Le Quere, C., Lima, I., Murtugudde, R., Shi, L., and Wetzel, P.: North Pacific carbon cycle response to climate variability on seasonal to decadal timescales, *J. Geophys. Res.*, 111, C07S06, doi:10.1029/2005JC003173, 2006.
- Metzl, N., Beauverger, C., Brunet, C., Goyet, C., and Poisson, A.: Surface water carbon dioxide in the southwest Indian Ocean sector of the Southern Ocean: A highly variable CO₂ source/sink region in summer, *Mar. Chem.*, 35, 85–95, 1991.
- Metzl, N., Poisson, A., Louanchi, F., Brunet, C., Sshauer, B., and Bres, B.: Spatio-temporal distributions of air–sea fluxes in the Indian and Antarctic oceans: A first step, *Tellus B*, 47, 56–69, 1995.
- Metzl, N., Louanchi, F., and Poisson, A. P.: Seasonal and interannual variations of sea surface carbon dioxide in the subtropical Indian Ocean, *Mar. Chem.*, 60, 131–146, 1998.
- Metzl, N.: Decadal increase of oceanic carbon dioxide in Southern Indian Ocean surface waters (1991–2007), *Deep-Sea Res. Pt. II*, 56, 607–619, 2009.
- Metzl, N., Tilbrook, B., and Poisson, A.: The annual fCO₂ cycle and the air–sea CO₂ flux in the sub-Antarctic Ocean, *Tellus B*, 51, 849–861, 1999.
- Mikaloff Fletcher, S. E., Gruber, N., Jacobson, A. R., Doney, S. C., Dutkiewicz, S., Gerber, M., Follows, M., Joos, F., Lindsay, K., Menemenlis, D., Mouchet, A., Muller, S. A., and Sarmiento, J. L.: Inverse estimates of anthropogenic CO₂ uptake, transport, and storage by the ocean, *Global Biogeochem. Cy.*, 20, GB2002, doi:10.1029/2005GB002530, 2006.
- Mikaloff Fletcher, S. E., Gruber, N., Jacobson, A. R., Gloor, M., Doney, S. C., Dutkiewicz, S., Gerber, M., Follows, M., Joos, F., Lindsay, K., Menemenlis, D., Mouchet, A., Muller, S. A., and Sarmiento, J. L.: Inverse estimates of the oceanic sources and sinks of natural CO₂ and the implied oceanic transport, *Global Biogeochem. Cy.*, 21, GB1010, doi:10.1029/2006GB002751, 2007.
- Miyama, T., Kominami, Y., Tamai, K., Nobuhiro, T., and Goto, Y.: Automated foliage chamber method for long-term measurement of CO₂ flux in the uppermost canopy, *Tellus B*, 55, 322–330, 2003.
- Murtugudde, R. and Busalacchi, A. J.: Interannual variability of the dynamics and thermo dynamics of the tropical Indian Ocean, *J. Clim.*, 12, 2300–2326, 1999.
- Murtugudde, R., Beauchamp, J., McClain, C. R., Lewis, M., and Busalacchi, A. J.: Effects of penetrative radiation on the upper tropical ocean circulation, *J. Climate*, 15, 470–486, 2002.
- Niwa, Y., Machida, T., Sawa, Y., Matsueda, H., Schuck, T. J., Breninkmeijer, C. A. M., Imasu, R., and Satoh, M.: Imposing strong constraints on tropical terrestrial CO₂ fluxes using passenger aircraft based measurements, *J. Geophys. Res.*, 117, D11303, doi:10.1029/2012JD017474, 2012.
- Patra, P. K., Maksyutov, S., Ishizawa, M., Nakazawa, T., Takahashi, T., and Ukita, J.: Interannual and decadal changes in the sea–air CO₂ flux from atmospheric CO₂ inverse modeling, *Global Biogeochem. Cy.*, 19, GB4013, doi:10.1029/2004GB002257, 2005.
- Patra, P. K., Gurney, K. R., Denning, A. S., Maksyutov, S., Nakazawa, T., Baker, D., Bousquet, P., Bruhwiler, L., Chen, Y. H., Ciais, P., Fan, S. M., Fung, I., Gloor, M., Heimann, M., Higuchi, K., John, J., Law, R. M., Maki, T., Pak, B. C., Peylin, P., Prather, M., Rayner, P. J., Sarmiento, J., Taguchi, S., Takahashi, T., and Yuen, C. W.: Sensitivity of inverse estimation of annual mean CO₂ sources and sinks to ocean-only sites versus all-sites observational networks, *Geophys. Res. Lett.*, 33, L05814, doi:10.1029/2005GL025403, 2006.
- Peters, W., Jacobson, A. R., Sweeney, C., Andrews, A. E., Conway, T. J., Masarie, K., Miller, J. B., Bruhwiler, L. M. P., Petron, G.,

- Hirsch, A. I., Worthy, D. E. J., van der Werf, G. R., Randerson, J. T., Wennberg, P. O., Krol, M. C., and Tans, P. P.: An atmospheric perspective on North American carbon dioxide exchange: Carbon Tracker, *Proc. Natl. Acad. Sci. USA*, 104, 18925–18930, doi:10.1073/pnas.0708986104, 2007.
- Peters, W., Krol, M. C., van der Werf, G. R., Houweling, S., Jones, C. D., Hughes, J., Schaefer, K., Masarie, K. A., Jacobson, A. R., Miller, J. B., Cho, C. H., Ramonet, M., Schmidt, M., Ciattaglia, L., Apadula, F., Helta, D., Meinhardt, F., di Sarra, A. G., Piacentino, S., Sferlazzo, D., Aalto, T., Hatakka, J., Strom, J., Haszpra, L., Meijer, H. A. J., van der Laan, S., Neubert, R. E. M., Jordan, A., Rodo, X., Morgui, J. A., Vermeulen, A. T., Popa, E., Rozanski, K., Zimnoch, M., Manning, A. C., Leuenberger, M., Uglietti, C., Dolman, A. J., Ciais, P., Heimann, M., and Tans, P. P.: Seven years of recent European net terrestrial carbon dioxide exchange constrained by atmospheric observations, *Global Change Biol.*, 16, 1317–1337, 2010.
- Pfeil, B., Olsen, A., Bakker, D. C. E., Hankin, S., Koyuk, H., Kozyr, A., Malczyk, J., Manke, A., Metzl, N., Sabine, C. L., Akl, J., Alin, S. R., Bates, N., Bellerby, R. G. J., Borges, A., Boutin, J., Brown, P. J., Cai, W.-J., Chavez, F. P., Chen, A., Cosca, C., Fassbender, A. J., Feely, R. A., González-Dávila, M., Goyet, C., Hales, B., Hardman-Mountford, N., Heinze, C., Hood, M., Hoppema, M., Hunt, C. W., Hydes, D., Ishii, M., Johannessen, T., Jones, S. D., Key, R. M., Körtzinger, A., Landschützer, P., Lauvset, S. K., Lefèvre, N., Lenton, A., Lourantou, A., Merlivat, L., Midorikawa, T., Mintrop, L., Miyazaki, C., Murata, A., Nakadate, A., Nakano, Y., Nakaoka, S., Nojiri, Y., Omar, A. M., Padin, X. A., Park, G.-H., Paterson, K., Perez, F. F., Pierrot, D., Poisson, A., Ríos, A. F., Santana-Casiano, J. M., Salisbury, J., Sarma, V. V. S. S., Schlitzer, R., Schneider, B., Schuster, U., Sieger, R., Skjelvan, I., Steinhoff, T., Suzuki, T., Takahashi, T., Tedesco, K., Telszewski, M., Thomas, H., Tilbrook, B., Tjiputra, J., Vandemark, D., Veness, T., Wanninkhof, R., Watson, A. J., Weiss, R., Wong, C. S., and Yoshikawa-Inoue, H.: A uniform, quality controlled Surface Ocean CO₂ Atlas (SOCAT), *Earth Syst. Sci. Data*, 5, 125–143, doi:10.5194/essd-5-125-2013, 2013.
- Piao, S. L., Ciais, P., Friedlingstein, P., Noblet-Ducoudre, N., Cadule, P., Viovy, N., and Wang, T.: Spatio-temporal patterns of terrestrial carbon cycle during the 20th century, *Global Biogeochem. Cy.*, 23, GB4026, doi:10.1029/2008GB003339, 2009.
- Poisson, A., Metzl, N., Brunet, C., Schauer, B., Bres, B., Ruizpino, D., and Louanchi, F.: Variability of sources and sinks of CO₂ in the Western Indian and Southern Oceans during the year 1991, *J. Geophys. Res.*, 98, 22759–22778, 1993.
- Raupach, M. R., Marland, G., Ciais, P., Le Quere, C., Canadell, J. G., Kleppe, G., and Field, C. B.: Global and regional drivers of accelerating CO₂ emissions, *P. Natl. A. Sci. USA*, 104, 10288–10293, 2007.
- Rayner, P. J., Law, R. M., Allison, C. E., Francey, R. J., Trudinger, C. M., and Pickett-Heaps, C.: Interannual variability of the global carbon cycle (1992–2005) inferred by inversion of atmospheric CO₂ and $\delta^{13}\text{C}$ measurements, *Global Biogeochem. Cy.*, 22, GB3008, doi:10.1029/2007GB003068, 2008.
- Sabine, C. L., Wanninkhof, R., Key, R. M., Goyet, C., and Millero, F. J.: Seasonal CO₂ fluxes in the tropical and subtropical Indian Ocean, *Mar. Chem.*, 72, 33–53, 2000.
- Sabine, C. L., Key, R. M., Johnson, K. M., Millero, F. J., Poisson, A., Sarmiento, J. L., Wallace, D. W. R., and Winn, C. D.: Anthropogenic CO₂ inventory of the Indian Ocean, *Global Biogeochem. Cy.*, 13, 179–198, 1999.
- Saji, N. H., Goswami, B. N., Vinayachandran, P. N., and Yamagata, T.: A dipole mode in the tropical Indian Ocean, *Nature*, 401, 360–363, 1999.
- Sarma, V. V. S. S., Kumar, M. D., George, M. D., and Rajendran, A.: Seasonal variations in inorganic carbon components in the central and eastern Arabian Sea, *Curr. Sci.*, 71, 852–856, 1996.
- Sarma, V. V. S. S., Kumar, M. D., and George, M. D.: The central and eastern Arabian Sea as a perennial source of atmospheric carbon dioxide, *Tellus B*, 50, 179–184, 1998.
- Sarma, V. V. S. S., Kumar, M. D., Gauns, M., and Madhupratap, M.: Seasonal controls on surface *p*CO₂ in the central and eastern Arabian Sea, *P. Indian A. Sci. (Earth Planet. Sci.)*, 109, 471–479, 2000.
- Sarma, V. V. S. S., Swati, P. S., Kumar, M. D., Kumar, S. P., Madhupratap, M., Ramaswamy, V., Sarin, M. M., Gauns, M., Bhattathiri, P. M. A., and Ramaiah, N.: Carbon budgets for the eastern and central Arabian Sea, *Global Biogeochem. Cy.*, 17, 1102, doi:10.1029/2002GB001978, 2003.
- Sarma, V. V. S. S.: Net oxygen production rates in the Arabian Sea using Modular Ocean Model, *Global Biogeochem. Cy.*, 18, GB4001, doi:10.1029/2003GB002198, 2004.
- Sarma, V. V. S. S.: Monthly variability in the surface *p*CO₂ and net air-sea CO₂ flux in the Arabian sea, *J. Geophys. Res.*, 108, 3255, doi:10.1029/2001JC001062, 2003.
- Sarma, V. V. S. S.: The influence of Indian Ocean Dipole (IOD) on biogeochemistry of carbon in the Arabian Sea during 1997–1998, *J. Earth Sys. Sci.*, 115, 433–450, 2006.
- Sarma, V. V. S. S., Krishna, M. S., Rao, V. D., Viswanadham, R., Kumar, N. A., Kumari, T. R., Gawade, L., Ghatkar, S., and Tari, A.: Sources and sinks of CO₂ in the west coast of Bay of Bengal, *Tellus B*, 64, 10961, doi:10.3402/tellusb.v64i0.10961, 2012.
- Schuster, U., McKinley, G. A., Bates, N., Chevallier, F., Doney, S. C., Fay, A. R., González-Dávila, M., Gruber, N., Jones, S., Krijnen, J., Landschützer, P., Lefèvre, N., Manizza, M., Mathis, J., Metzl, N., Olsen, A., Ríos, A. F., Rödenbeck, C., Santana-Casiano, J. M., Takahashi, T., Wanninkhof, R., and Watson, A. J.: An assessment of the Atlantic and Arctic sea-air CO₂ fluxes, 1990–2009, *Biogeosciences*, 10, 607–627, doi:10.5194/bg-10-607-2013, 2013.
- Schott, F. A. and McCreary, J. P.: The monsoon circulation of the Indian Ocean, *Prog. Oceanogr.*, 51, 1–123, 2001.
- Schott, F. A., Dengler, M., and Schoenefeldt, R.: The shallow overturning circulation of the Indian Ocean, *Prog. Oceanogr.*, 53, 57–103, 2002.
- Schott, F. A., Xie, S. P., and McCreary Jr., J. P.: Indian Ocean circulation and climate variability, *Rev. Geophys.*, 47, RG1002, doi:10.1029/2007RG000245, 2009.
- Sengupta, D., Bharath Raj, G. N., and Sheno, S. S.: Surface freshwater from Bay of Bengal runoff and Indonesian Through flow in the tropical Indian Ocean, *Geophys. Res. Lett.*, 33, L22609, doi:10.1029/2006GL027573, 2006.
- Sweeney, C., Gloor, E., Jacobson, A. R., Key, R. M., KcKinley, G., Sarimento, J. L., and Wanninkhof, R.: Constraining global air-sea gas exchange for CO₂ with recent bomb 14C measurements, *Global Biogeochem. Cy.*, 21, GB2015, doi:10.1029/2006GB002784, 2007.

- Takahashi, T., Wanninkhof, R. H., Feely, R. A., Weiss, R. F., Chipman, D. W., Bates, N., Olafsson, J., Sabine, C., and Sutherland, S. C.: Net sea-air CO₂ flux over the global oceans: An improved estimate based on the sea-air *p*CO₂ difference, in Second International Symposium, CO₂ in the Oceans, Extended Abstracts, Center Global Env. Res, Tsukuba, Japan, 9–15, 1999.
- Takahashi, T., Sutherland, S. C., Sweeney, C., Poisson, A., Metzl, N., Tilbrook, B., Bates, N., Wanninkhof, R., Feely, R. A., Sabine, C., Olafsson, J., and Nojiri, Y.: Global sea-air CO₂ flux based on climatological surface ocean *p*CO₂, and seasonal biological and temperature effects, *Deep-Sea Res.*, II, 49, 1601–1622, 2002.
- Takahashi, T., Sutherland, S. C., Wanninkhof, R., Sweeney, C., Feely, R. A., Chipman, D. W., Hales, B., Friederich, G., Chavez, F., Sabine, C., Watson, A., Bakker, D. C. E., Schuster, U., Metzl, N., Yoshikawa-Inoue, H., Ishii, M., Midorikawa, T., Nojiri, Y., Kortzinger, A., Steinhoff, T., Hoppema, M., Olafsson, J., Arnarson, T. S., Tilbrook, B., Johannessen, T., Olsen, A., Bellerby, R., Wong, C. S., Delille, B., Bates, N. R., and de Baar, H. J. W.: Climatological mean and decadal change in surface ocean *p*CO₂ and net sea-air CO₂ flux over the global oceans, *Deep-Sea Res. Pt. II*, 56, 554–577, 2009.
- Thompson, D. W. J. and Solomon, S.: Interpretation of recent Southern Hemisphere climate change, *Science*, 296, 895–899, 2002.
- Thomas, H., Prowe, A. E. F., Lima, I. D., Doney, S. C., Wanninkhof, R., Greatbatch, R. J., Schuster, U., and Corbiere, A.: Changes in the North Atlantic Oscillation influence CO₂ uptake in the North Atlantic over the past 2 decades, *Global Biogeochem. Cy.*, 22, Gb4027, doi:10.1029/2007gb003167, 2008.
- Valsala, V. and Ikeda, M.: Pathways and effects of the Indonesian Through flow water in the Indian Ocean using Particle trajectory and Tracers in an OGCM, *J. Climate*, 20, 2994–3017, 2007.
- Valsala, V., Maksyutov, S., and Murtugudde, R.: Possible interannual to interdecadal variabilities of the Indonesian through flow water pathways in the Indian Ocean, *J. Geophys. Res.*, 115, C10016, doi:10.1029/2009JC005735, 2010a.
- Valsala, V. and Maksyutov, S.: Inter-annual variability of the air-sea CO₂ flux in the north Indian Ocean, *Ocean Dynam.*, 63, 165–178, 2013.
- Valsala, V., Maksyutov, S., and Murtugudde, R.: A window for carbon uptake in the southern subtropical Indian Ocean, *Geophys. Res. Lett.*, 39, L17605, doi:10.1029/2012GL052857, 2012.
- Wanninkhof, R., Park, G.-H., Takahashi, T., Sweeney, C., Feely, R., Nojiri, Y., Gruber, N., Doney, S. C., McKinley, G. A., Lenton, A., Le Quéré, C., Heinze, C., Schwinger, J., Graven, H., and Khaliwala, S.: Global ocean carbon uptake: magnitude, variability and trends, *Biogeosciences*, 10, 1983–2000, doi:10.5194/bg-10-1983-2013, 2013.
- Wyrtki, K.: Physical oceanography of the Indian Ocean, in *Ecological studies: Analysis and Synthesis*, edited by: Zeitzschel, B., Springer-Verlag, New York, 3, 18–36, 1973.
- Xie, S. P., Annamalai, H., Schott, F. A., McCreary, J. P.: Structure and mechanisms of South Indian Ocean climate variability, *J. Climate*, 15, 864–878, 2002.